

What Does It Take to Induce Equilibrium in Bidirectional Energy Transfers?

Di Gao, Shawkat M. Aly, Paul-Ludovic Karsenti, and Pierre D. Harvey

Table of Content

	Page
Figure S1. ^1H NMR spectrum of 3 in CD_2Cl_2 .	3
Figure S2. ^1H NMR spectrum of 4 in CD_2Cl_2 .	3
Figure S3. ^1H NMR spectrum of 5 in CD_2Cl_2 .	4
Figure S4. ^1H NMR spectrum of 1 in CD_2Cl_2 .	4
Figure S5. ^1H NMR spectrum of 1 in CD_2Cl_2 .	5
Figure S6. ^1H NMR spectrum of 2 in CD_2Cl_2 .	5
Figure S7. ^1H NMR spectrum of 2 in CD_2Cl_2 .	6
Figure S8. MALDI-TOF spectrum of 3 .	6
Figure S9. MALDI-TOF spectrum of 4 .	7
Figure S10. MALDI-TOF spectrum of 5 .	7
Figure S11. MALDI-TOF spectrum of 1 .	8
Figure S12. MALDI-TOF spectrum of 2 .	8
Figure S13. Absorption, fluorescence, and excitation spectra of 5 , 8 , 9 , 1 and 2 in 2MeTHF at 77K	9
Figure S14. Decay of emission intensity (black), fit (red), IRF (blue), residual (green) and lifetime distribution (orange) of 5 . Left, at 298 K, $\lambda = 675$ nm, $\tau_e \{B\} = 2.05$ ns {0.0192}, $\chi^2 = 1.09$. Right, at 77 K, $\lambda = 443$ nm, $\tau_e \{B\} = 2.51$ ns {0.0118}, $\chi^2 = 1.04$.	10
Figure S15. Decay of emission intensity (black), fit (red), IRF (blue), residual (green) and lifetime distribution (orange) of 8 . Left, at 298 K, $\lambda = 666$ nm, $\tau_e \{B\} = 10.81$ ns {0.0712}, $\chi^2 = 1.09$. Right, at 77 K, $\lambda = 662$ nm, $\tau_e \{B\} = 12.88$ ns {0.0677}, $\chi^2 = 1.09$.	10
Figure 16. Decay of emission intensity (black), fit (red), IRF (blue), residual (green) and lifetime distribution (orange) of 9 . Left, at 298 K, $\lambda = 739$ nm, $\tau_e \{B\} = 11.05$ ns {0.0712}, $\chi^2 = 1.08$. Right, at 77 K, $\lambda = 648$ nm, $\tau_e \{B\} = 13.42$ ns {0.0696}, $\chi^2 = 1.06$.	10
Figure 17. Decay of emission intensity (black), fit (red), IRF (blue), residual (green) and lifetime distribution (orange) of 1 . Left, at 298 K, $\lambda = 671$ nm, $\tau_e \{B\} = 1.86$ ns {0.0161}, 5.30 ns {0.0008}, $\chi^2 = 1.05$. Right, at 77 K, $\lambda = 668$ nm, $\tau_e \{B\} = 0.11$ ns {0.0159}, 4.66 ns {0.0160} 8.91 ns {0.0250}, $\chi^2 = 1.00$.	11
Figure 18. Decay of emission intensity (black), fit (red), IRF (blue), residual (green) and lifetime distribution (orange) of 2 . Left, at 298 K, $\lambda = 657$ nm, $\tau_e \{B\} = 0.10$ ns {0.0123}, 3.06 ns {0.0606} 6.31 ns {0.0170}, $\chi^2 = 1.06$. Right, at 77 K, $\lambda = 668$ nm, $\tau_e \{B\} = 0.04$ ns {0.0695}, 2.71 ns {0.0202} 11.5 ns {0.0436}, $\chi^2 = 1.07$.	11
Figure S19. Geometry optimization of 1 (DFT; B3LYP). Left: side view; right: top view.	11
Figure S20. Representation of the frontier MOs of 1 . Energy in eV.	12
Table S1. Computed positions, major contributions and oscillator strength of the first 100 electronic transitions of 2 .	13
Figure S22. Geometry optimization of 2 . Top: side view; bottom: top view.	16

Figure S23. Representation of the frontier MOs of 2 .	17
Table S2. Computed positions, major contributions and oscillator strength of the first 100 electronic transitions of 2 .	18
Figure S24. Bar graph reporting the calculated oscillator strength and calculated position of the 100 st electronic transitions calculated by TDDFT for 2 .	20
Figure S25. Time evolution of 1 of the fs-TAS in 2MeTHF at 298 K.	21
Figure S26. Time evolution of $\Delta T/T$ for 1 in 2MeTHF at 298 K for various monitored wavelengths.	21
Figure S27. Time evolution of the fs-TAS 2 in 2MeTHF at 298 K.	22
Figure S28. Time evolution of $\Delta T/T$ for 2 in 2MeTHF at 298 K for various monitored wavelengths.	22
Figure S29. Time evolution of the fluorescence spectra of 1 in 2MeTHF at 298 K.	23
Figure S30. Time evolution of the fluorescence intensity of 1 in 2MeTHF at 298 K monitored at various wavelengths.	23
Figure S31. Time evolution of the fluorescence spectra of 1 in 2MeTHF at 77 K.	24
Figure S32. Time-deconvoluted spectra of 1 in 2 MeTHF at 77 K..	24
Figure S33. Time evolution of the fluorescence intensity of 1 in 2MeTHF at 77 K monitored at various wavelengths.	25
Figure S34. Time evolution of the fluorescence spectra of 2 in 2MeTHF at 298 K.	25
Figure S35. Time evolution of the fluorescence intensity of 2 in 2MeTHF at 298 K monitored at various wavelengths.	26
Figure S36. Time evolution of the fluorescence spectra of 2 in 2MeTHF at 77 K.	26
Figure S37. Time-deconvoluted spectra of 2 in 2-MeTHF at 77 K.	27
Figure S38. Time evolution of the fluorescence spectra of 2 in 2MeTHF at 77 K monitored at various wavelengths.	27
Figure 39. Sum of the absorption spectra of 5 + 8 , and 5 + 9 (top), compared to those for 1 and 2 .	28
Figure 40. Schematic representations of the four possible conformations of dyads 1 and 2 .	28

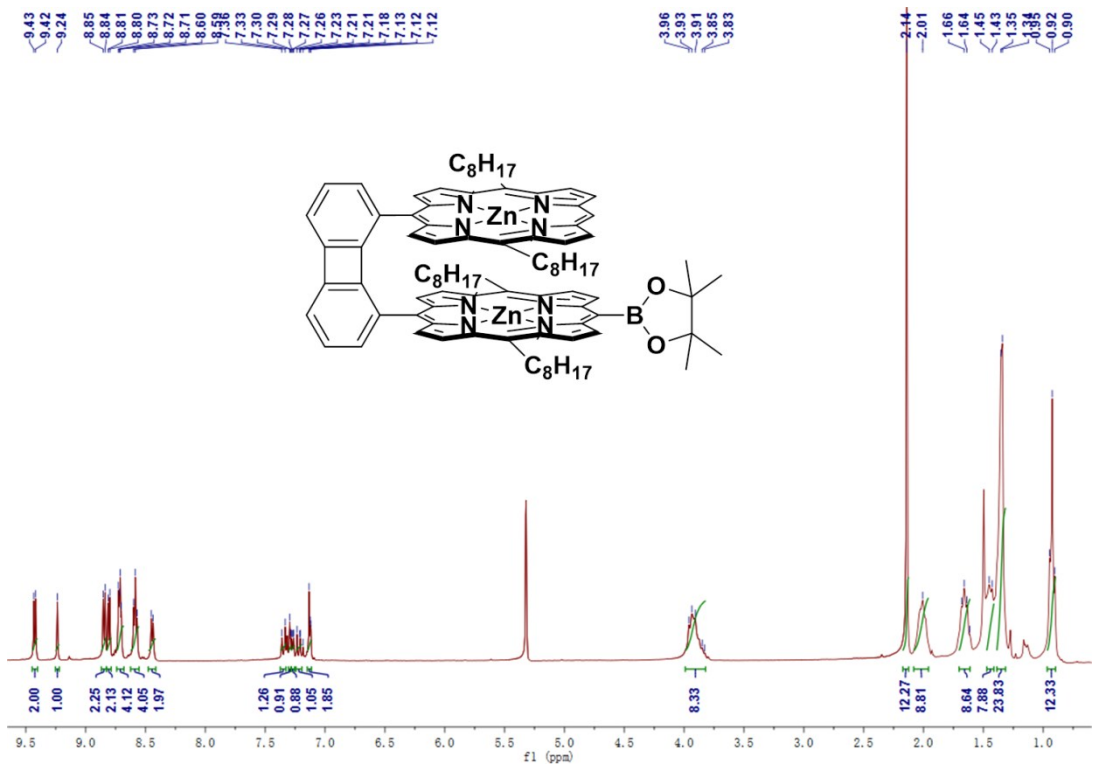


Figure S1. ^1H NMR spectrum of **3** in CD_2Cl_2 .

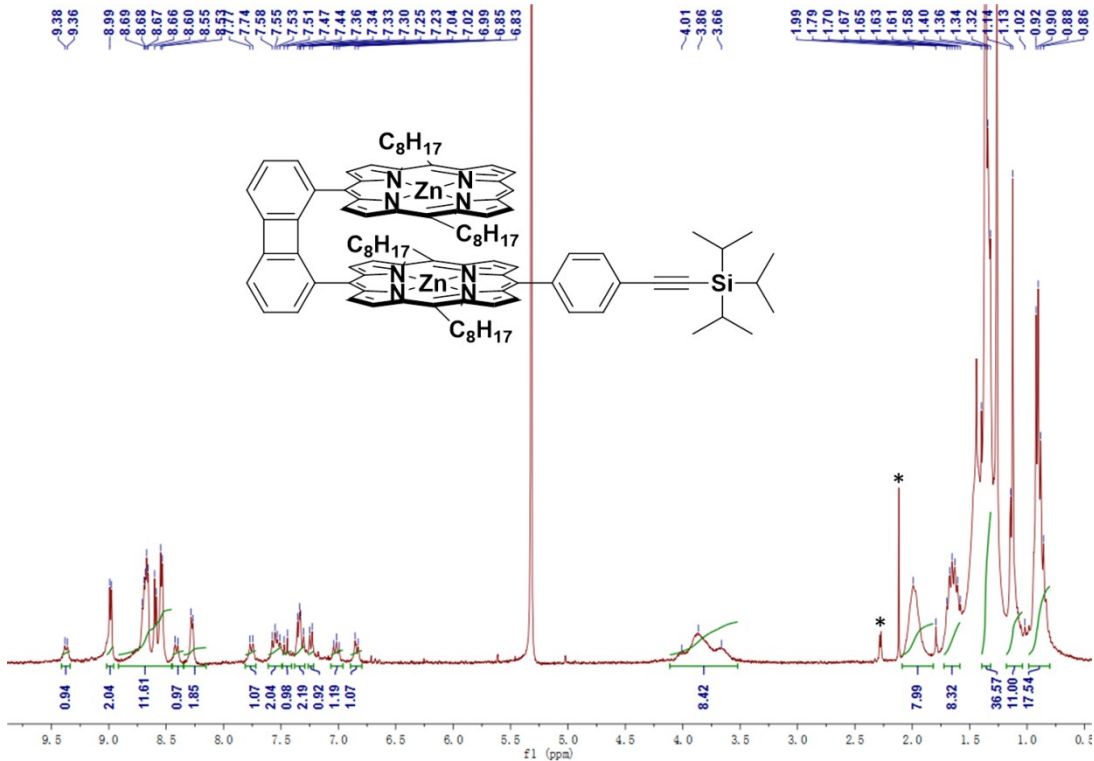


Figure S2. ^1H NMR spectrum of **4** in CD_2Cl_2 .

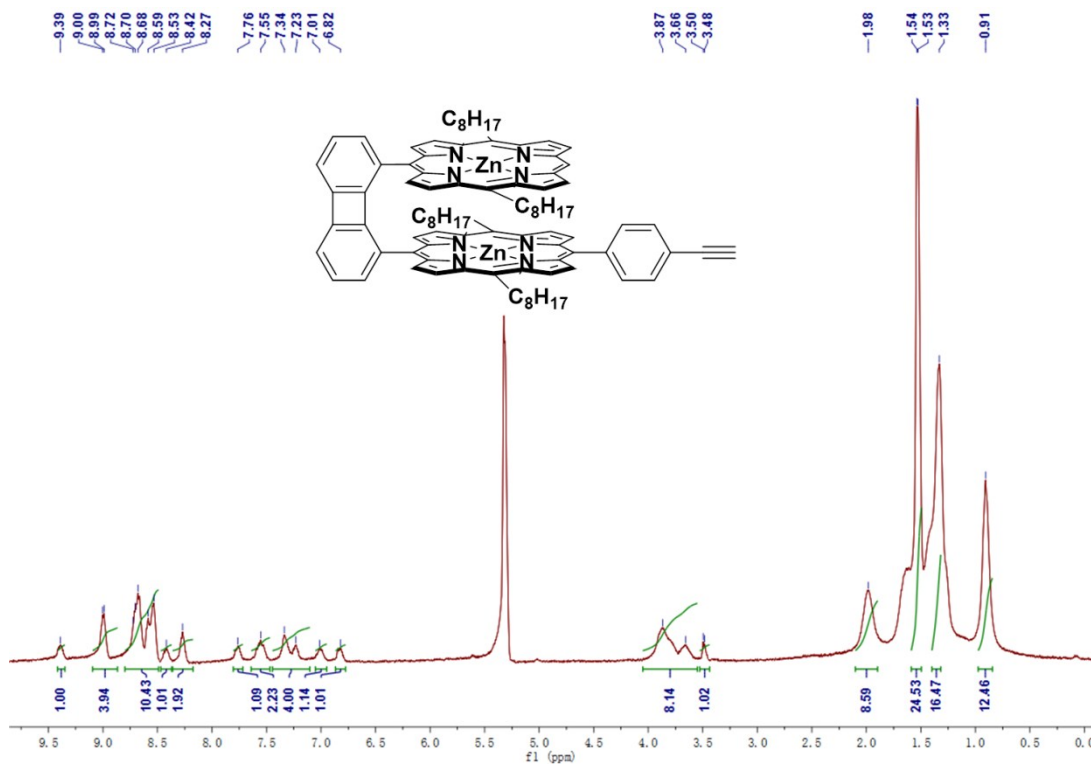


Figure S3. ^1H NMR spectrum of **5** in CD_2Cl_2 .

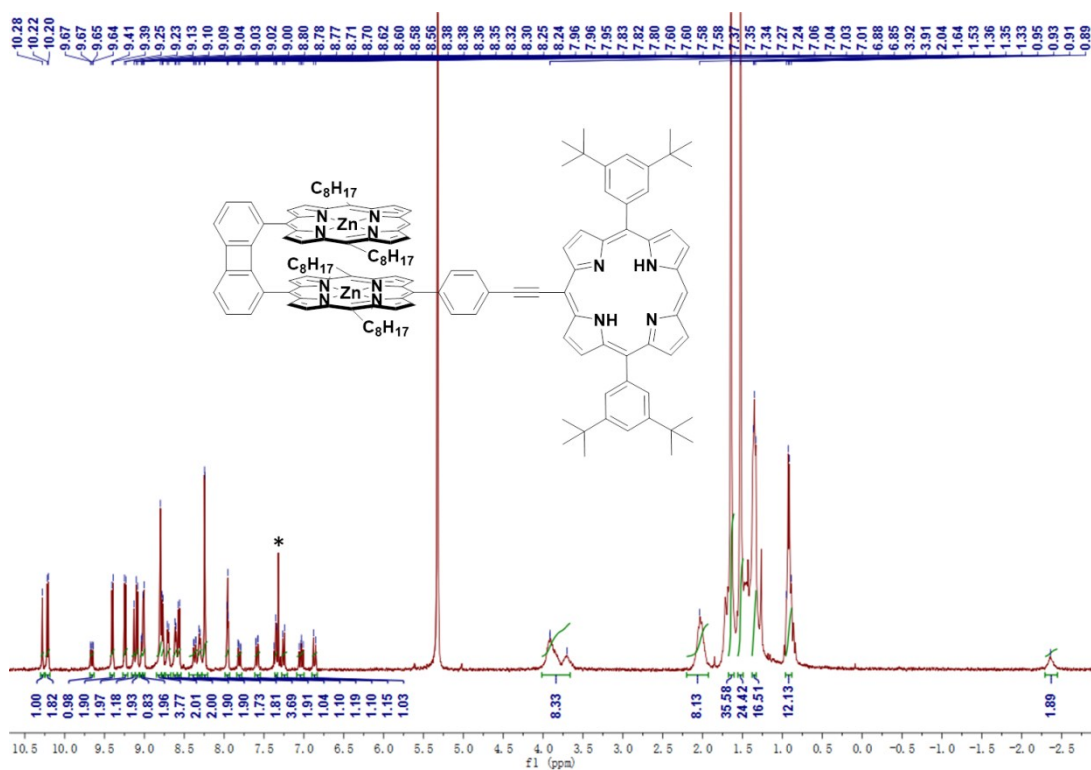


Figure S4. ^1H NMR spectrum of **1** in CD_2Cl_2 .

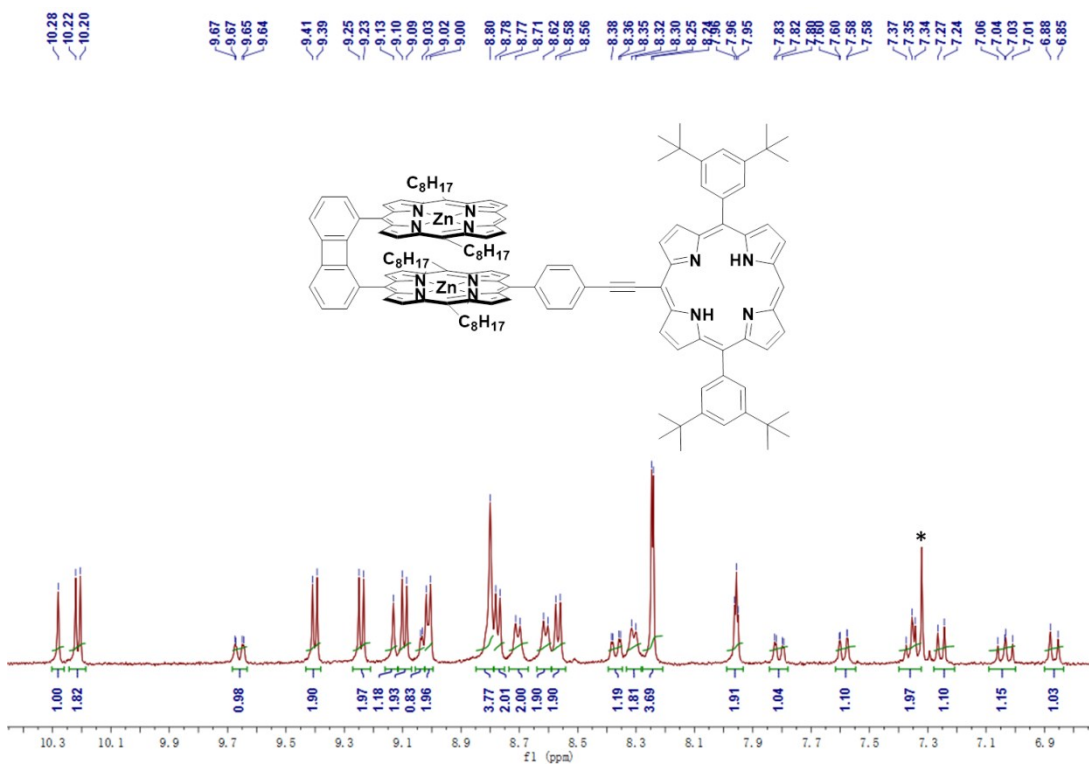


Figure S5. ¹H NMR spectrum of **1** in CD_2Cl_2 .

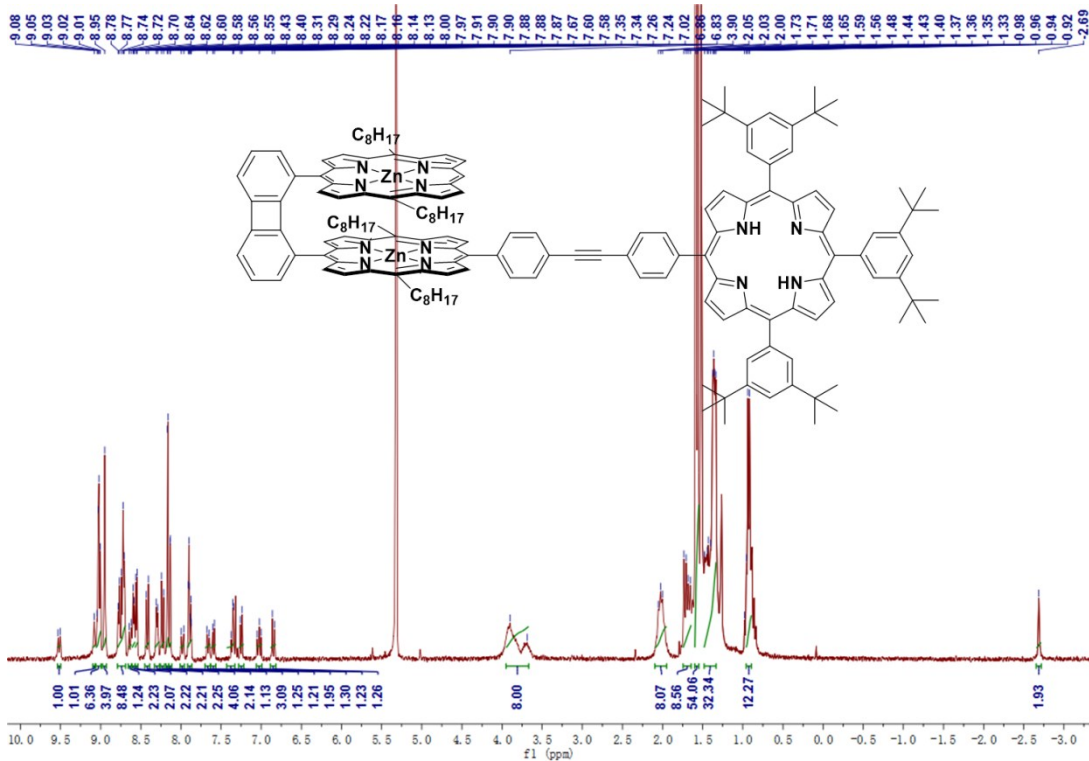


Figure S6. ¹H NMR spectrum of **2** in CD_2Cl_2 .

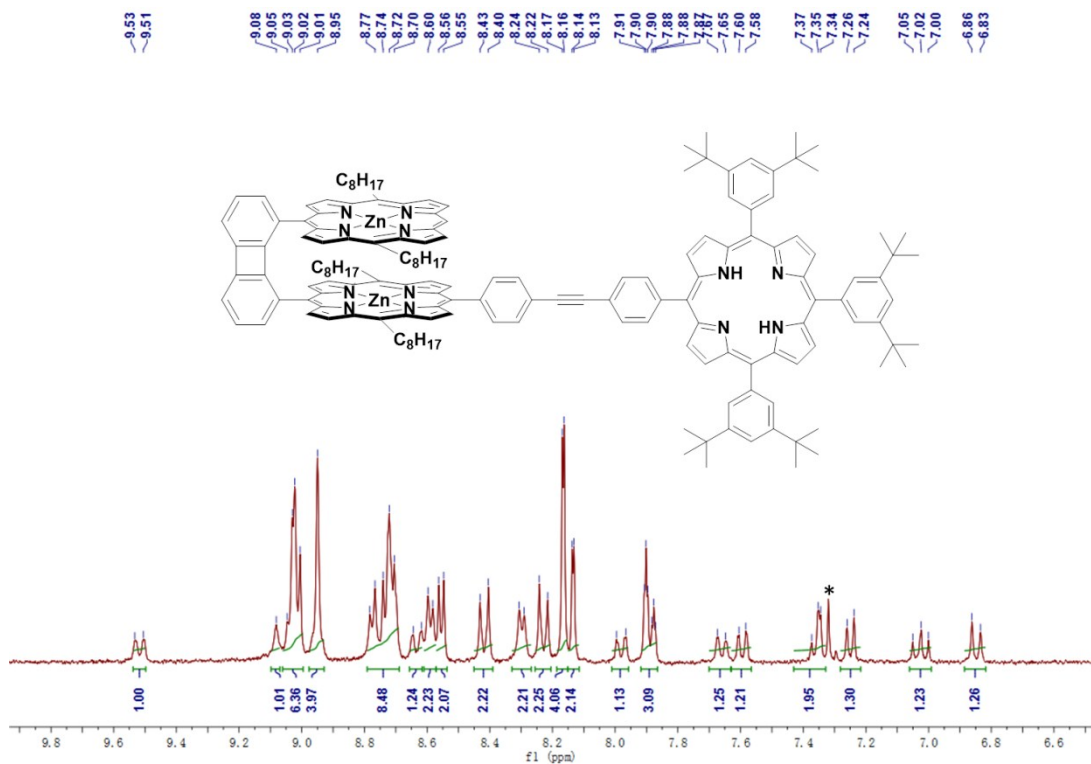


Figure S7. ^1H NMR spectrum of **2** in CD_2Cl_2 .

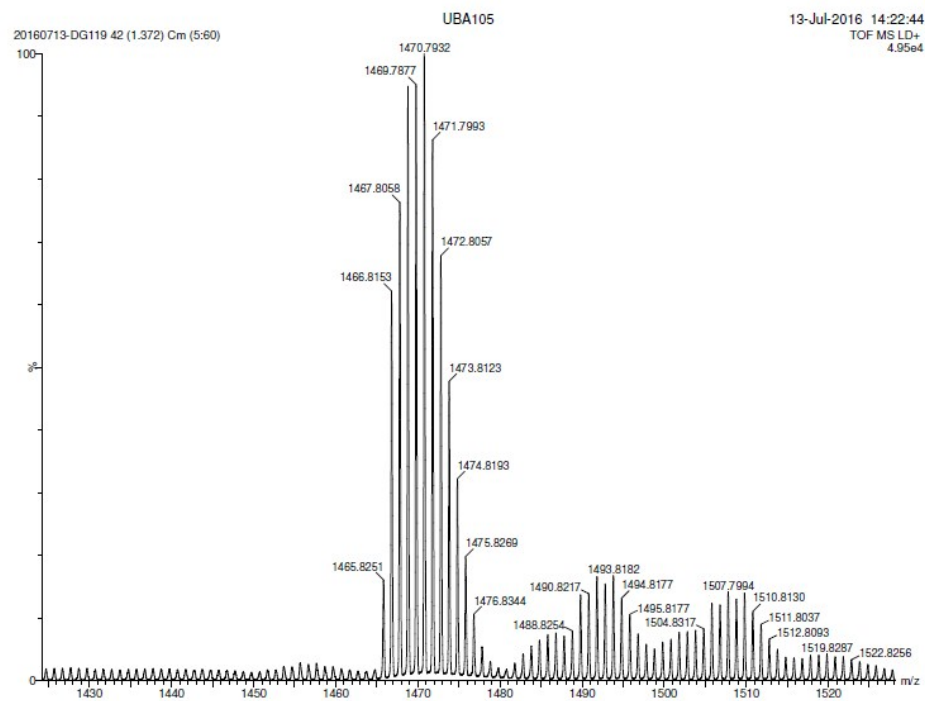


Figure S8. MALDI-TOF spectrum of **3**.

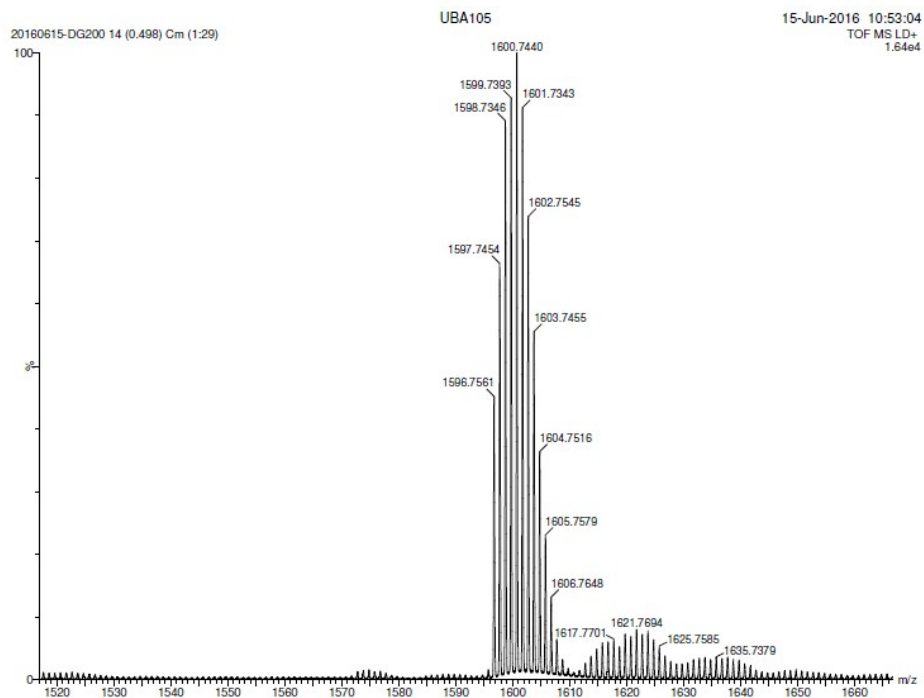


Figure S9. MALDI-TOF spectrum of **4**.

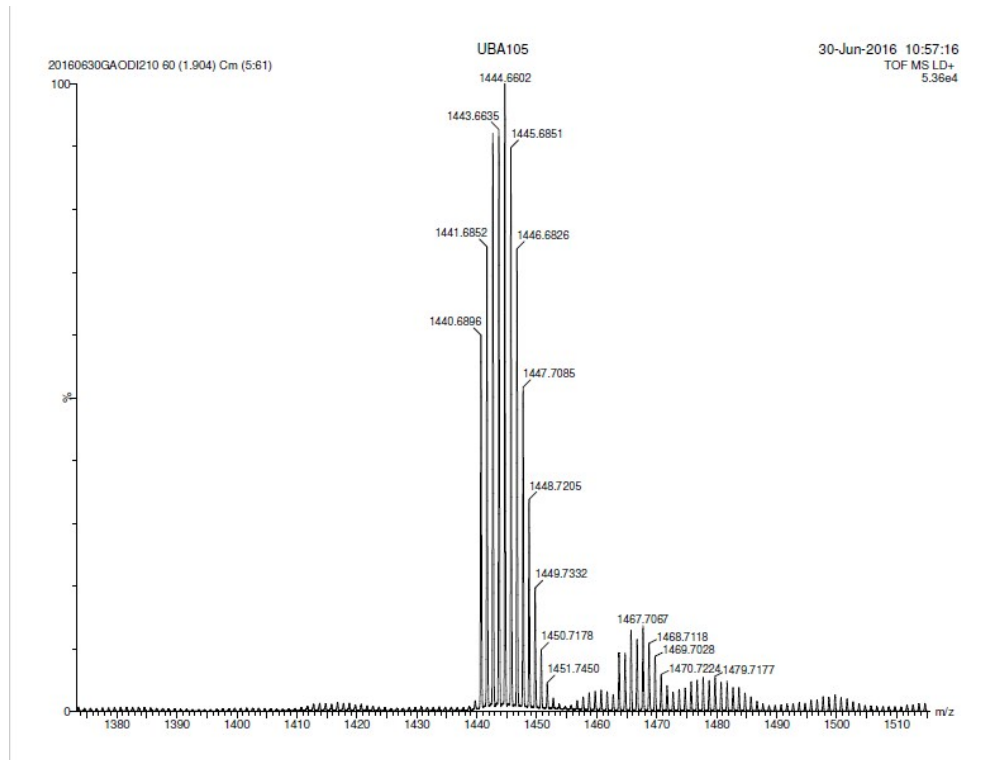


Figure S10. MALDI-TOF spectrum of **5**.

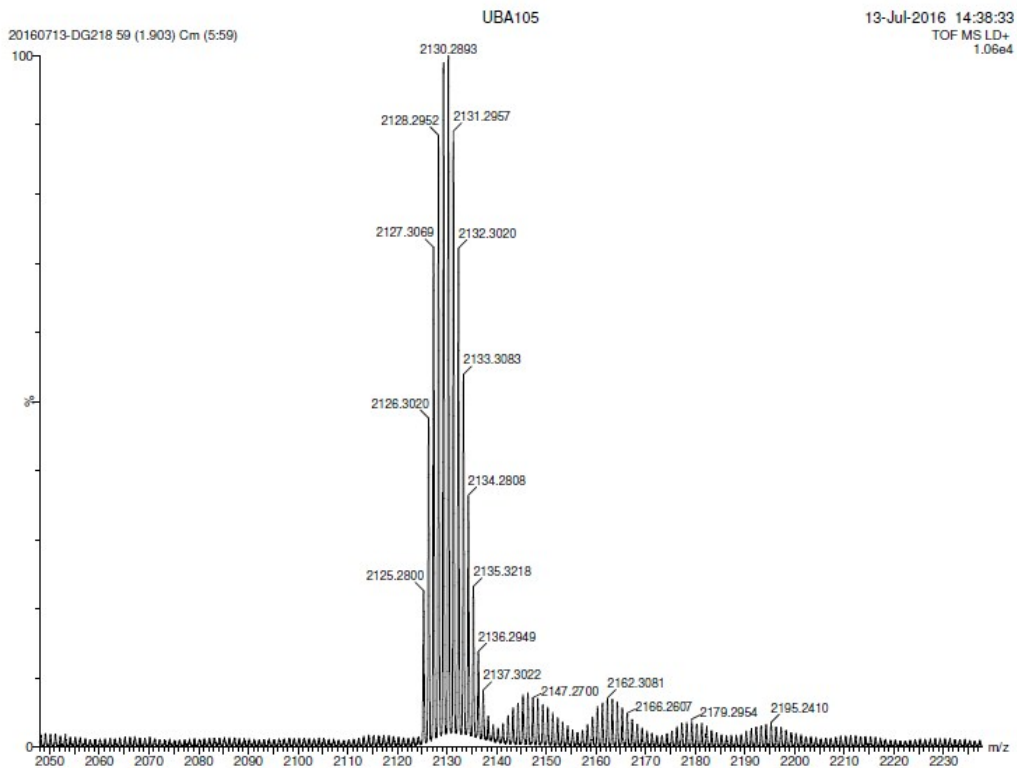


Figure S11. MALDI-TOF spectrum of **1**.

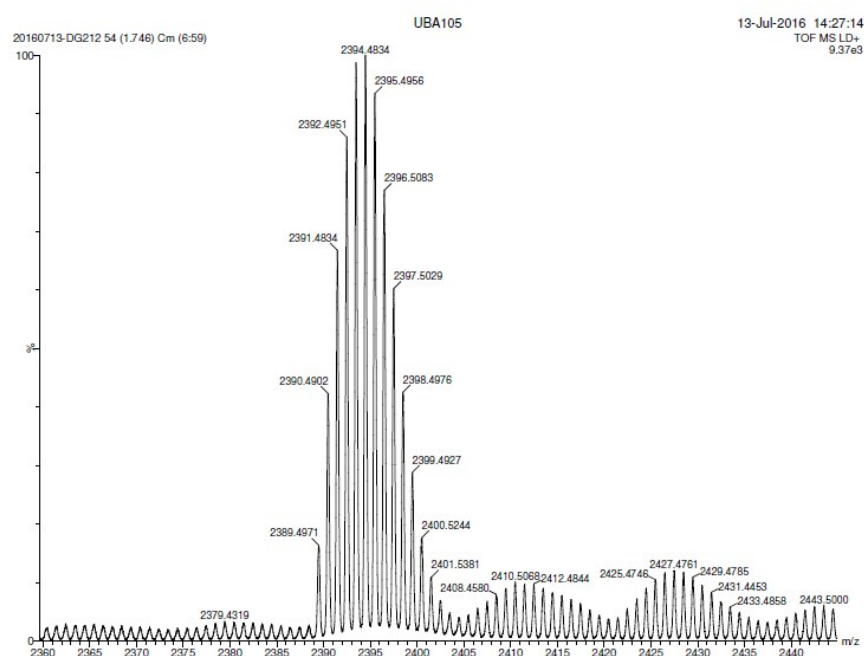


Figure S12. MALDI-TOF spectrum of **2**.

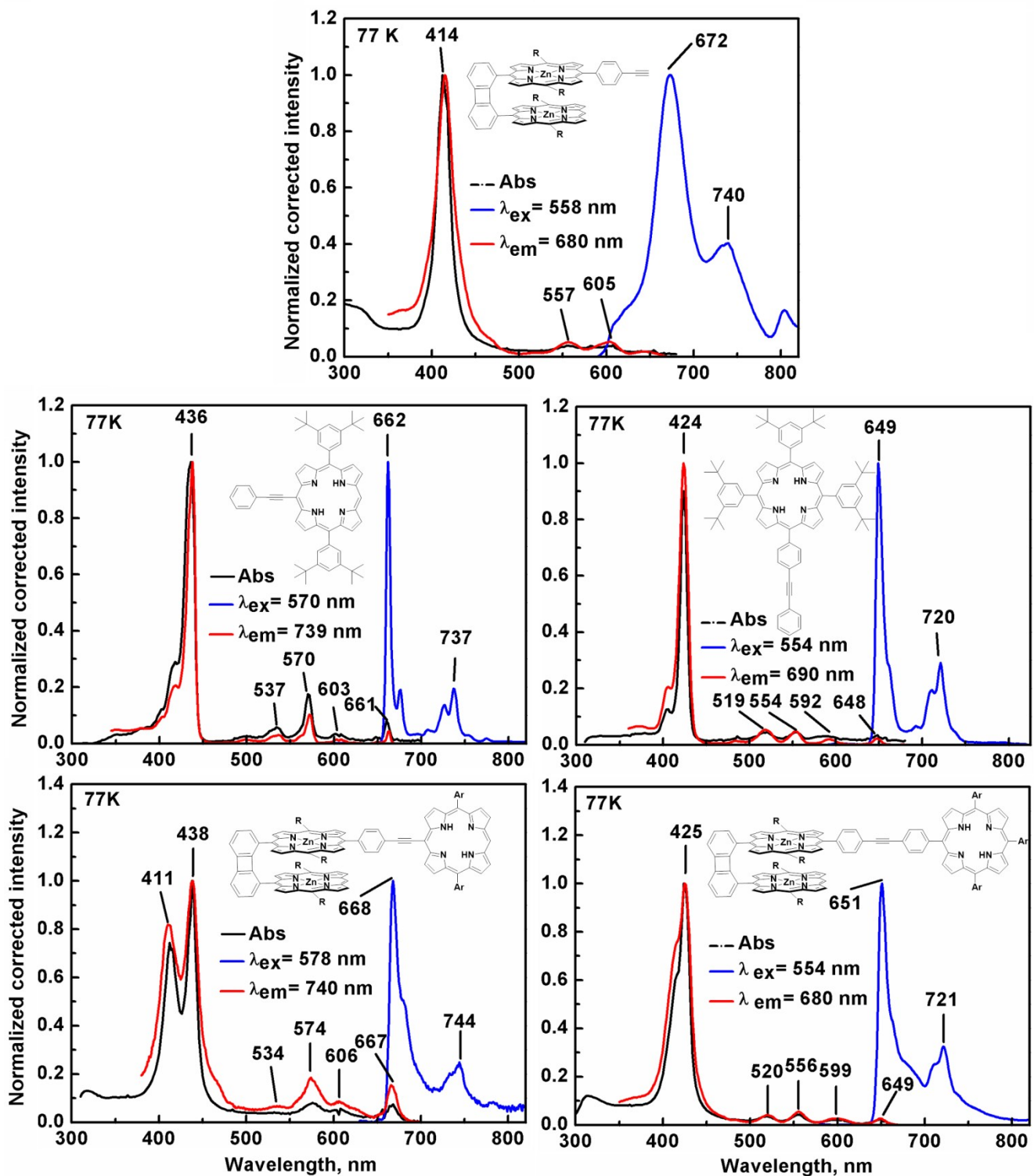


Figure S13. Absorption (black), fluorescence (blue), and excitation (red) spectra of **5**, **8**, **9**, **1** and **2** in 2MeTHF at 77 K (R = n-octyl, Ar = di-3,5-t-butylbenzene).

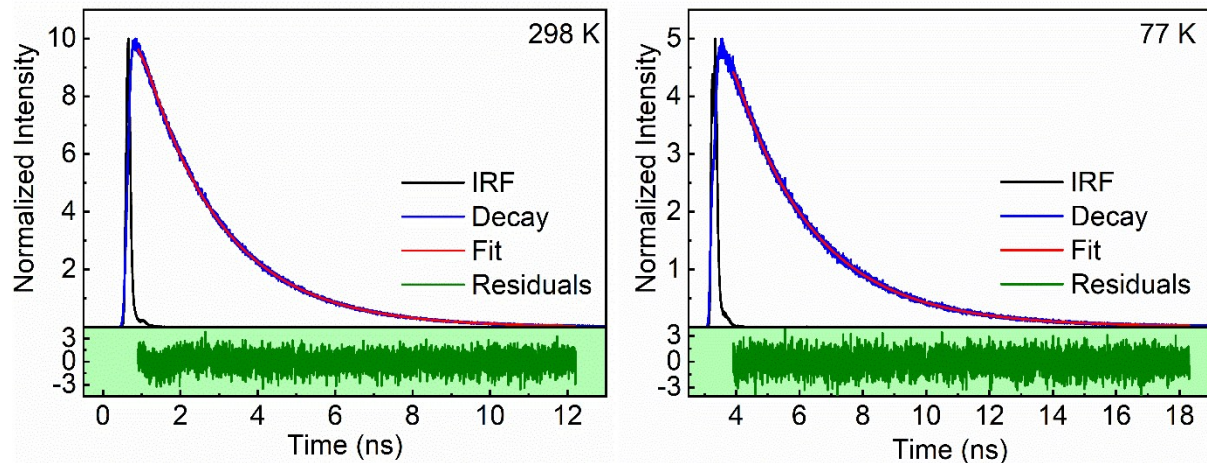


Figure S14. Decay of emission intensity (black), fit (red), IRF (blue), residual (green) and lifetime distribution (orange) of **5**. Left, at 298 K, $\lambda = 675$ nm, $\tau_e \{B\} = 2.05$ ns (standard deviation) {0.0192}, $\chi^2 = 1.09$. Right, at 77 K, $\lambda = 443$ nm, $\tau_e \{B\} = 2.51$ ns {0.0118} (0.150), $\chi^2 = 1.04$.

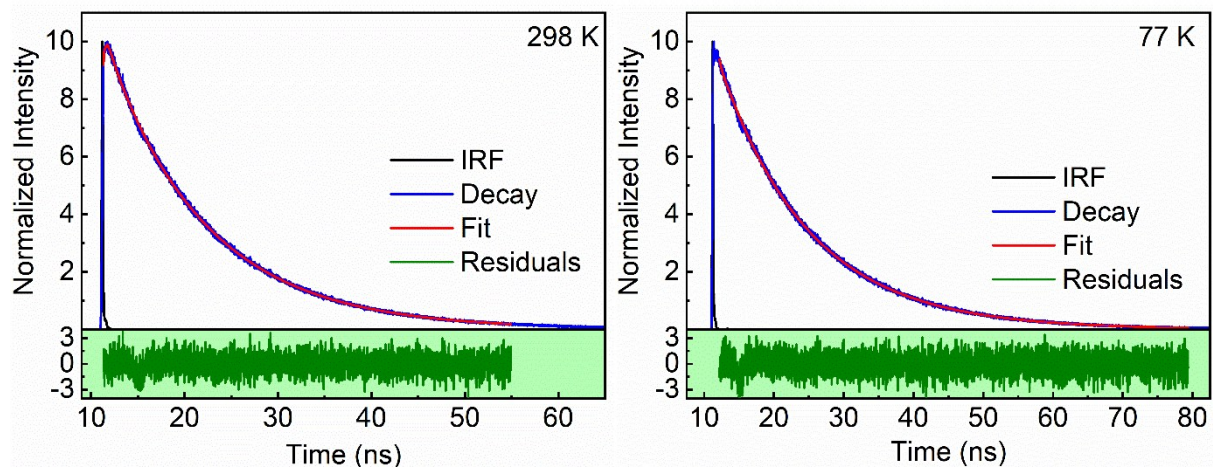


Figure S15. Decay of emission intensity (black), fit (red), IRF (blue), residual (green) and lifetime distribution (orange) of **8**. Left, at 298 K, $\lambda = 666$ nm, $\tau_e \{B\} = 10.81$ ns (standard deviation) {0.0712} (0.980), $\chi^2 = 1.09$. Right, at 77 K, $\lambda = 662$ nm, $\tau_e \{B\} = 12.88$ ns {0.0677} (0.841), $\chi^2 = 1.09$.

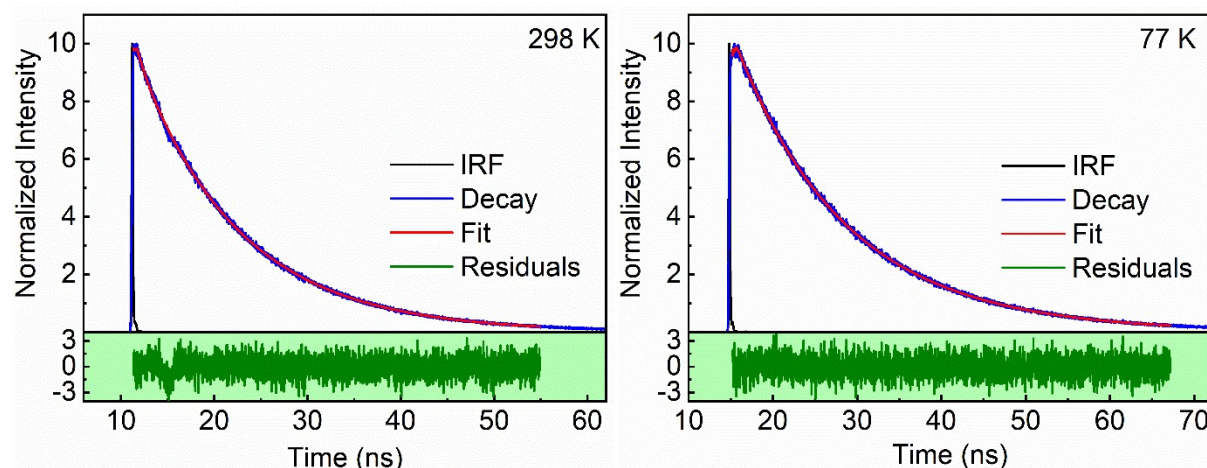


Figure 16. Decay of emission intensity (black), fit (red), IRF (blue), residual (green) and lifetime distribution (orange) of **9**. Left, at 298 K, $\lambda = 739$ nm, $\tau_e \{B\}$ (standard deviation) = 11.05 ns {0.0712} (1.056), $\chi^2 = 1.08$. Right, at 77 K, $\lambda = 648$ nm, $\tau_e \{B\} = 13.42$ ns {0.0696} (1.969), $\chi^2 = 1.06$.

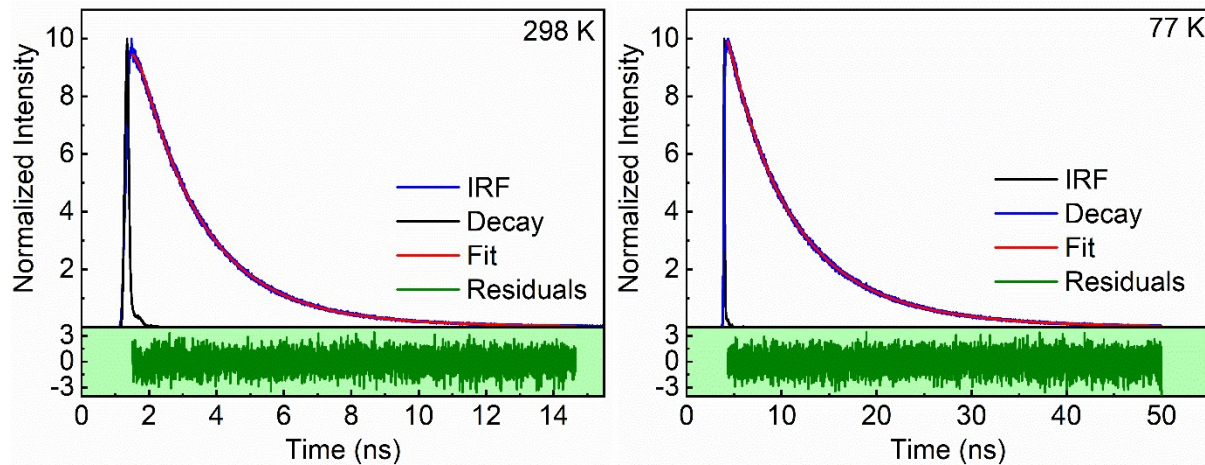


Figure 17. Decay of emission intensity (black), fit (red), IRF (blue), residual (green) and lifetime distribution (orange) of **1**. Left, at 298 K, $\lambda = 671$ nm, $\tau_e \{B\} = 1.86$ ns {0.0161}, 5.30 ns {0.0008}, $\chi^2 = 1.05$. Right, at 77 K, $\lambda = 668$ nm, $\tau_e \{B\}$ (standard deviation) = 0.11 ns {0.0159} (0.003), 4.66 ns {0.0160} (0.255) 8.91 ns {0.0250} (0.686), $\chi^2 = 1.00$.

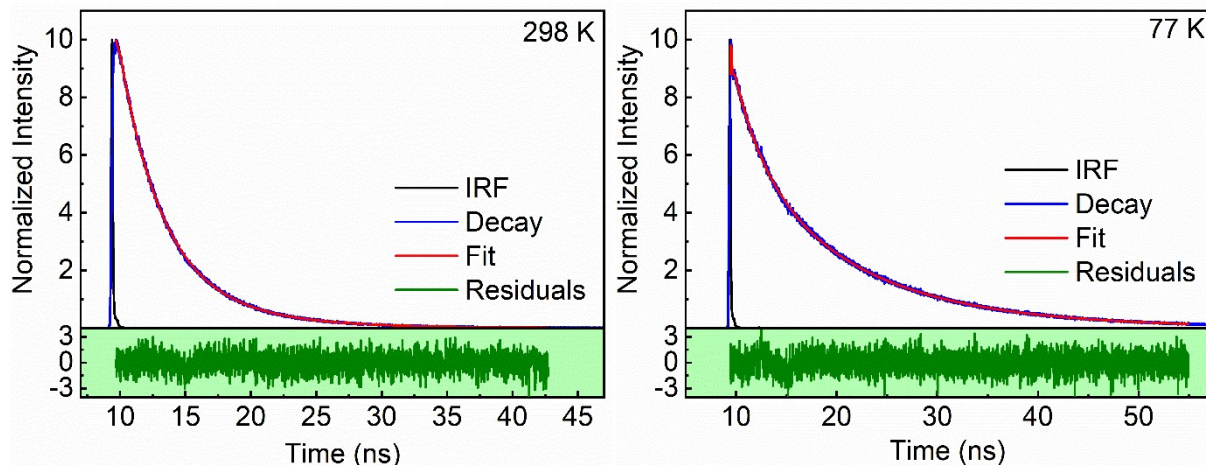


Figure 18. Decay of emission intensity (black), fit (red), IRF (blue), residual (green) and lifetime distribution (orange) of **2**. Left, at 298 K, $\lambda = 657$ nm, $\tau_e \{B\} = 0.10$ ns {0.0123}, 3.06 ns {0.0606} 6.31 ns {0.0170}, $\chi^2 = 1.06$. Right, at 77 K, $\lambda = 668$ nm, $\tau_e \{B\}$ (standard deviation) = 0.04 ns {0.0695} (0.005), 2.71 ns {0.0202} (0.401), 11.5 ns {0.0436} (2.728), $\chi^2 = 1.07$.

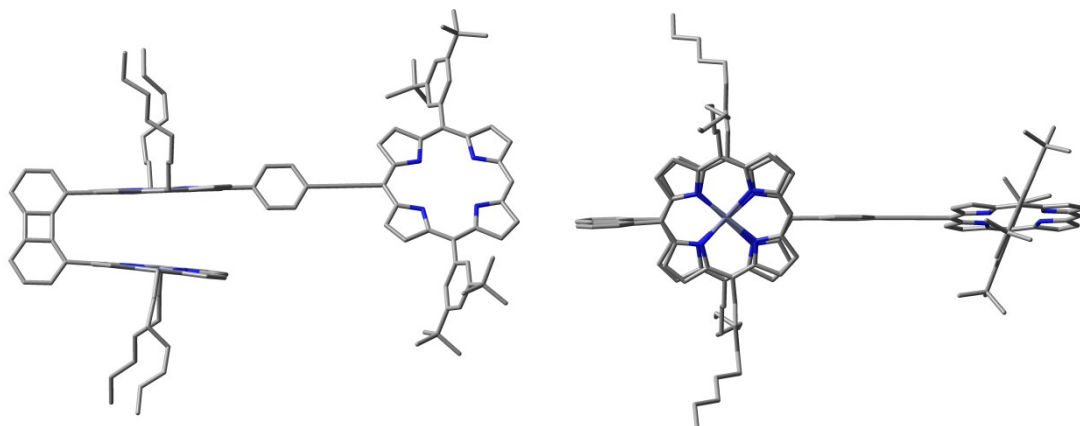


Figure S19. Geometry optimization of **1** (DFT; B3LYP). Left: side view; right: top view. The interplanar dihedral angles and centre-to-centre distances are placed in the text.

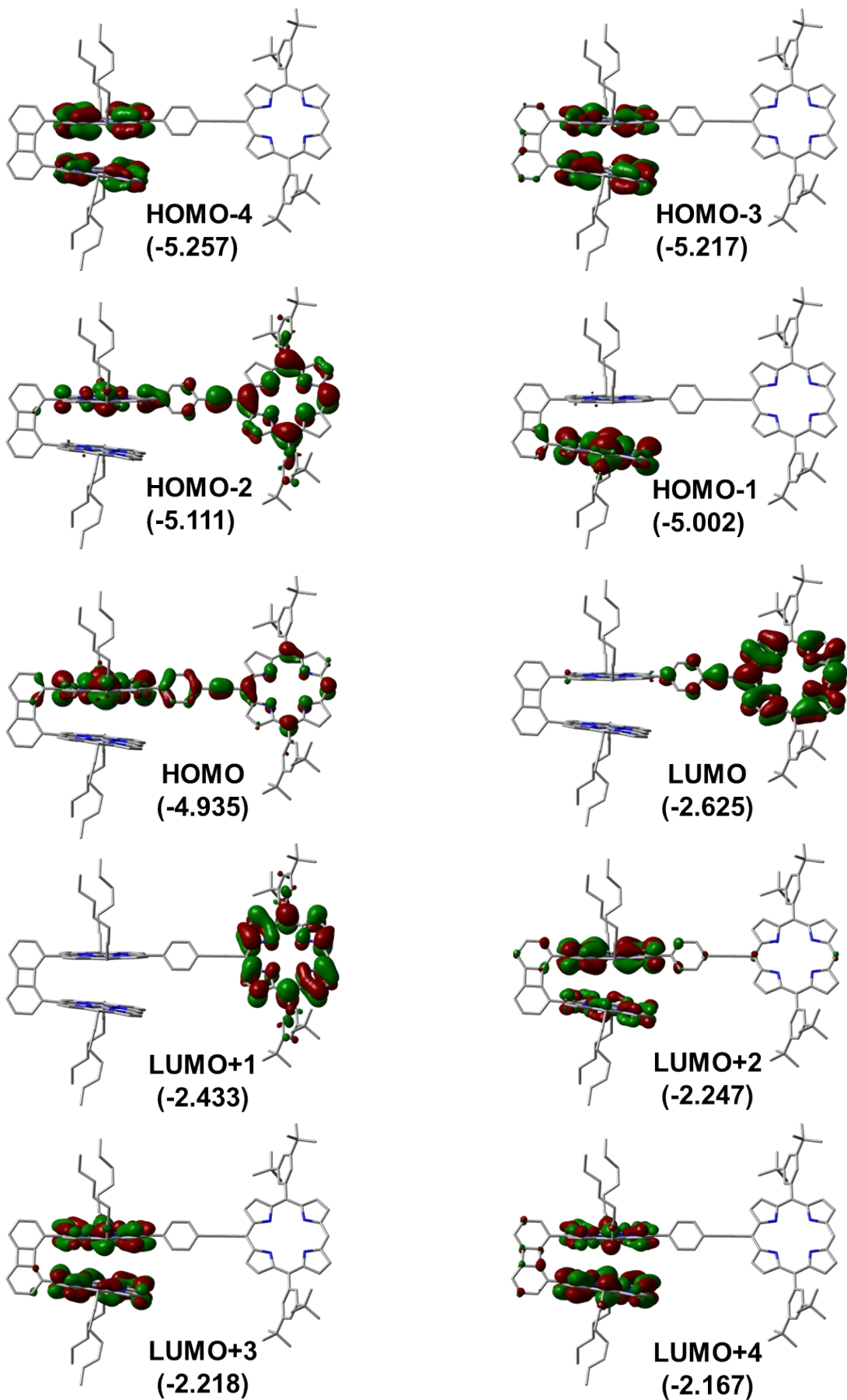


Figure S20. Representation of the frontier MOs of **1**. Energy in eV.

Table S1. Computed positions, major contributions and oscillator strength (f) of the first 100 electronic transitions of **1** (H = HOMO, L = LUMO).

No.	Wavelength (nm)	Osc. Strength	Major Contribs (%)
1	609.8	0.3197	H-5→LUMO (11), H-5→L+1 (10), HOMO→LUMO (48), HOMO→L+1 (15)
2	584.1	0.2139	H-5→LUMO (17), H-2→L+1 (11), HOMO→LUMO (36), HOMO→L+1 (25)
3	559.9	0.0083	H-1→LUMO (52), H-1→L+2 (12)
4	556.1	0.0167	H-2→LUMO (43)
5	549.8	0.0039	H-1→LUMO (25), HOMO→L+2 (20), HOMO→L+3 (18)
6	545.7	0.0066	H-2→LUMO (20), H-1→L+3 (16), HOMO→L+2 (12), HOMO→L+3 (15)
7	543.5	0.0016	H-1→L+2 (11), HOMO→L+2 (11), HOMO→L+4 (22)
8	539.2	0.0014	H-1→L+3 (14), H-1→L+4 (20), HOMO→L+5 (16)
9	533.5	0.003	H-1→L+2 (23), HOMO→L+3 (15), HOMO→L+4 (19)
10	529.8	0.0043	H-2→L+5 (10), H-1→L+3 (16), HOMO→L+4 (14), HOMO→L+5 (35)
11	520.5	0.003	H-1→L+2 (10), H-1→L+3 (24), H-1→L+4 (38)
12	518.7	0.0054	H-1→L+2 (14), H-1→L+5 (57)
13	511.7	0.0042	H-4→LUMO (20), H-3→LUMO (60)
14	510.1	0.0026	H-2→L+1 (51), HOMO→L+1 (40)
15	504.0	0.0024	H-4→LUMO (61), H-3→LUMO (19)
16	500.2	0.0001	H-1→L+1 (95)
17	490.8	0.0951	H-2→L+2 (33), HOMO→L+2 (16)
18	487.5	0.011	H-4→L+3 (21), H-3→L+2 (10), H-3→L+4 (13), H-2→L+2 (16)
19	483.7	0.0007	H-4→L+2 (14), H-4→L+4 (34), H-3→L+3 (19), H-3→L+5 (23)
20	482.9	0.0045	H-4→L+5 (11), H-3→L+4 (15), H-2→L+2 (13), H-2→L+3 (24), HOMO→L+3 (10)
21	481.5	0.0049	H-4→L+2 (24), H-4→L+3 (10), H-3→L+3 (11), H-3→L+5 (16)
22	480.1	0.0047	H-4→L+5 (31), H-3→L+2 (10), H-3→L+4 (15), H-2→L+3 (26)
23	471.8	0.0005	H-2→L+4 (58), HOMO→L+4 (21)
24	468.1	0.0002	H-3→L+1 (97)
25	467.4	0.0181	H-2→L+5 (60), HOMO→L+5 (24)
26	461.8	0.0002	H-4→L+1 (97)
27	434.5	0.0167	H-6→LUMO (57), H-6→L+2 (29)
28	426.4	0.4091	H-6→LUMO (11), H-6→L+2 (18), H-6→L+3 (19), H-4→L+5 (10)
29	421.9	0.4676	H-6→L+3 (16), H-5→LUMO (18), H-5→L+2 (23)
30	419.6	0.1776	H-6→L+3 (24), H-6→L+4 (12), H-5→L+2 (20)
31	415.2	0.4267	H-6→LUMO (21), H-6→L+2 (27), H-6→L+3 (15)
32	414.5	0.3164	H-6→L+4 (61)
33	412.4	0.0247	H-5→L+2 (22), H-5→L+3 (72)
34	408.1	0.1204	H-6→L+2 (10), HOMO→L+6 (16)
35	407.1	0.052	H-6→L+5 (72)
36	405.8	0.0347	H-5→L+4 (75)
37	404.3	0.0971	H-5→L+4 (12), H-2→L+6 (10), HOMO→L+6 (25)
38	402.8	0.2523	H-5→L+5 (53)
39	400.2	0.2474	H-5→L+5 (22), H-1→L+6 (39)
40	399.1	0.3904	H-5→L+5 (14), H-1→L+6 (12)
41	397.5	0.0841	H-6→L+1 (90)
42	390.4	0.0249	H-1→L+6 (28), HOMO→L+6 (12)
43	382.7	0.2344	H-8→LUMO (48), H-7→LUMO (10)

44	378.1	0.135	H-8→LUMO (18), H-7→LUMO (38)
45	373.1	0.24	H-4→L+6 (21), H-3→L+6 (32)
46	371.9	0.2227	H-4→L+6 (22), H-3→L+6 (47)
47	367.2	0.2054	H-7→L+1 (23), H-4→L+6 (26), HOMO→L+7 (16)
48	366.3	0.0034	H-10→LUMO (11), H-10→L+2 (31), H-10→L+3 (13), H-9→L+2 (13)
49	364.1	1.0378	H-6→L+6 (14), H-4→L+3 (11), H-3→L+2 (14)
50	363.2	0.0799	H-11→L+2 (26), H-11→L+3 (30), H-11→L+5 (14)
51	361.4	0.0006	H-6→L+6 (10), H-2→L+6 (56), HOMO→L+6 (22)
52	360.7	0.0578	H-10→L+3 (16), H-10→L+4 (19), H-10→L+5 (13)
53	360.2	0.2798	H-7→L+1 (10), H-4→L+6 (14)
54	359.8	0.0256	H-11→L+2 (15), H-11→L+3 (12), H-11→L+4 (30), H-11→L+5 (19)
55	358.0	0.0774	H-13→LUMO (24), H-12→LUMO (15), H-7→L+1 (12), HOMO→L+7 (14)
56	357.1	0.4059	H-6→L+6 (50), H-2→L+6 (10)
57	356.6	0.0075	H-8→L+1 (67)
58	351.4	0.0055	H-2→L+8 (12), HOMO→L+7 (15), HOMO→L+8 (42)
59	348.2	0.0019	H-16→LUMO (11), H-15→LUMO (76)
60	347.1	0.0042	H-14→LUMO (11), H-14→L+2 (16), H-9→L+2 (13)
61	346.2	0.0119	H-19→LUMO (17), H-1→L+8 (15)
62	345.5	0.021	H-1→L+7 (11), H-1→L+8 (41)
63	344.8	0.0056	H-19→LUMO (49)
64	343.8	0.2201	H-13→L+1 (21), H-12→L+1 (13)
65	342.0	0.2086	H-13→L+1 (13), HOMO→L+7 (13)
66	341.8	0.0192	H-12→L+2 (15)
67	340.2	0.0203	H-16→LUMO (12), H-13→LUMO (10), H-12→LUMO (14)
68	338.5	0.0111	H-7→L+2 (14), H-2→L+7 (17)
69	338.3	0.0108	H-15→L+1 (14), H-2→L+7 (10)
70	338.0	0.0037	H-20→LUMO (31), H-15→L+1 (31)
71	337.6	0.0001	H-11→LUMO (70)
72	336.9	0.0118	H-20→LUMO (58), H-15→L+1 (23)
73	335.7	0.0004	H-9→LUMO (19), H-7→L+2 (18), H-2→L+7 (12)
74	334.7	0.0061	H-14→LUMO (20), H-7→L+3 (10), H-1→L+7 (23)
75	334.5	0.0008	H-1→L+7 (42), H-1→L+8 (10)
76	334.1	0.0027	H-10→LUMO (53), H-9→LUMO (11)
77	333.4	0.003	H-7→L+2 (13)
78	332.7	0.0299	H-12→L+3 (21)
79	331.8	0.0036	H-19→L+1 (29), H-16→LUMO (19)
80	331.7	0.0156	H-19→L+1 (30), H-7→L+2 (10)
81	331.4	0.0061	H-19→L+1 (11), H-7→L+3 (11)
82	330.9	0.0077	H-7→L+2 (10), H-7→L+3 (19)
83	330.2	0.0109	H-17→LUMO (26), H-17→L+2 (13)
84	329.4	0.0194	H-3→L+7 (24), H-3→L+8 (57)
85	329.2	0.0093	H-14→L+2 (12), H-7→L+4 (13)
86	328.6	0.0024	H-10→L+3 (25), H-10→L+4 (16)
87	328.2	0.0409	H-14→L+2 (12)
88	327.1	0.0279	H-14→L+2 (12)
89	327.1	0.0001	H-7→L+4 (10), H-7→L+5 (19)
90	326.6	0.005	H-10→L+4 (12), H-10→L+5 (17), H-9→L+5 (11)

91	326.5	0.0065	H-20→L+1 (34), H-10→L+5 (13)
92	326.3	0.012	H-20→L+1 (19), H-11→L+4 (13), H-11→L+5 (11), H-4→L+8 (24)
93	326.3	0.0078	H-11→L+3 (13), H-11→L+4 (20), H-11→L+5 (19), H-4→L+8 (18)
94	326.1	0.0051	H-20→L+1 (20), H-18→LUMO (20), H-4→L+8 (10)
95	325.2	0.0018	H-14→L+3 (11), H-7→L+4 (30)
96	324.9	0.0001	H-11→LUMO (16), H-11→L+2 (31), H-11→L+3 (12), H-11→L+5 (19)
97	324.4	0.0002	H-17→LUMO (20), H-9→L+4 (10)
98	323.8	0.0044	H-14→L+2 (14)
99	323.3	0.0046	H-7→L+5 (28)
100	322.8	0.0056	HOMO→L+9 (54)

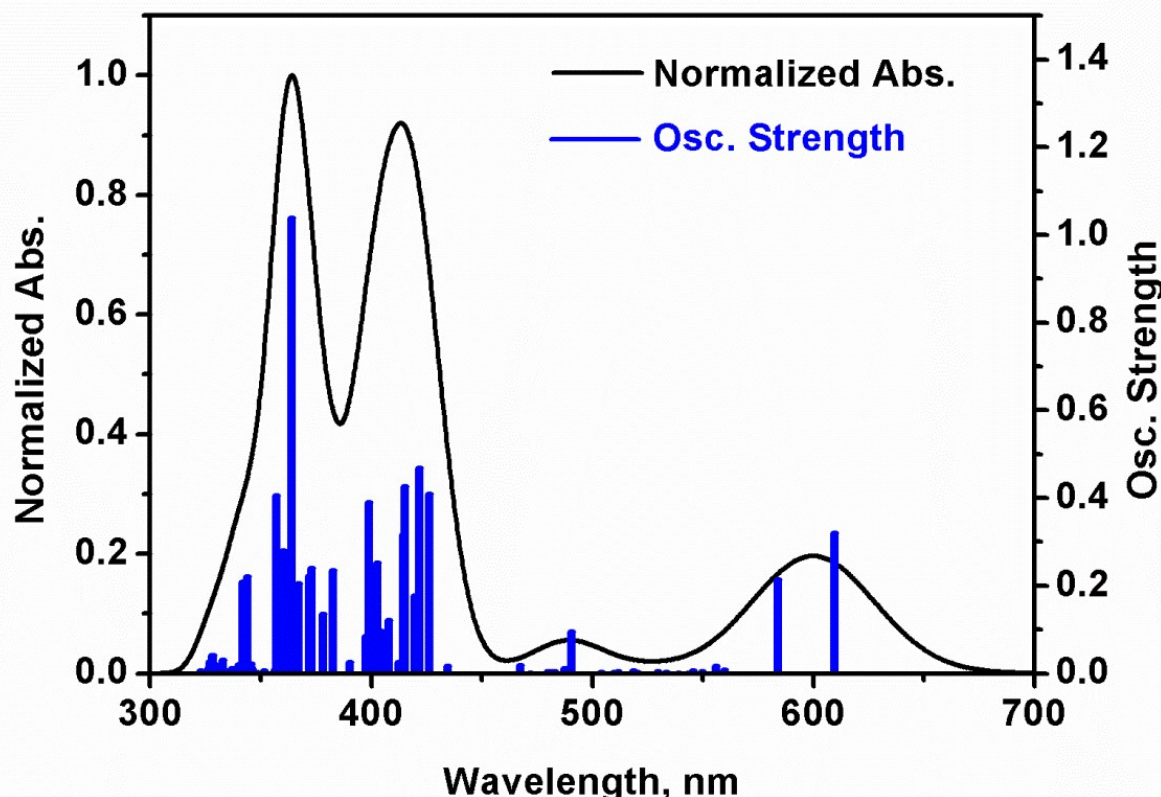


Figure S21. Bar graph reporting the calculated oscillator strength and calculated position of the 100st electronic transitions calculated by TDDFT for **1** (bar graph; f = computed oscillator strength). The black line is generated by assigning an arbitrary thickness of 1000 cm⁻¹ to each bar.

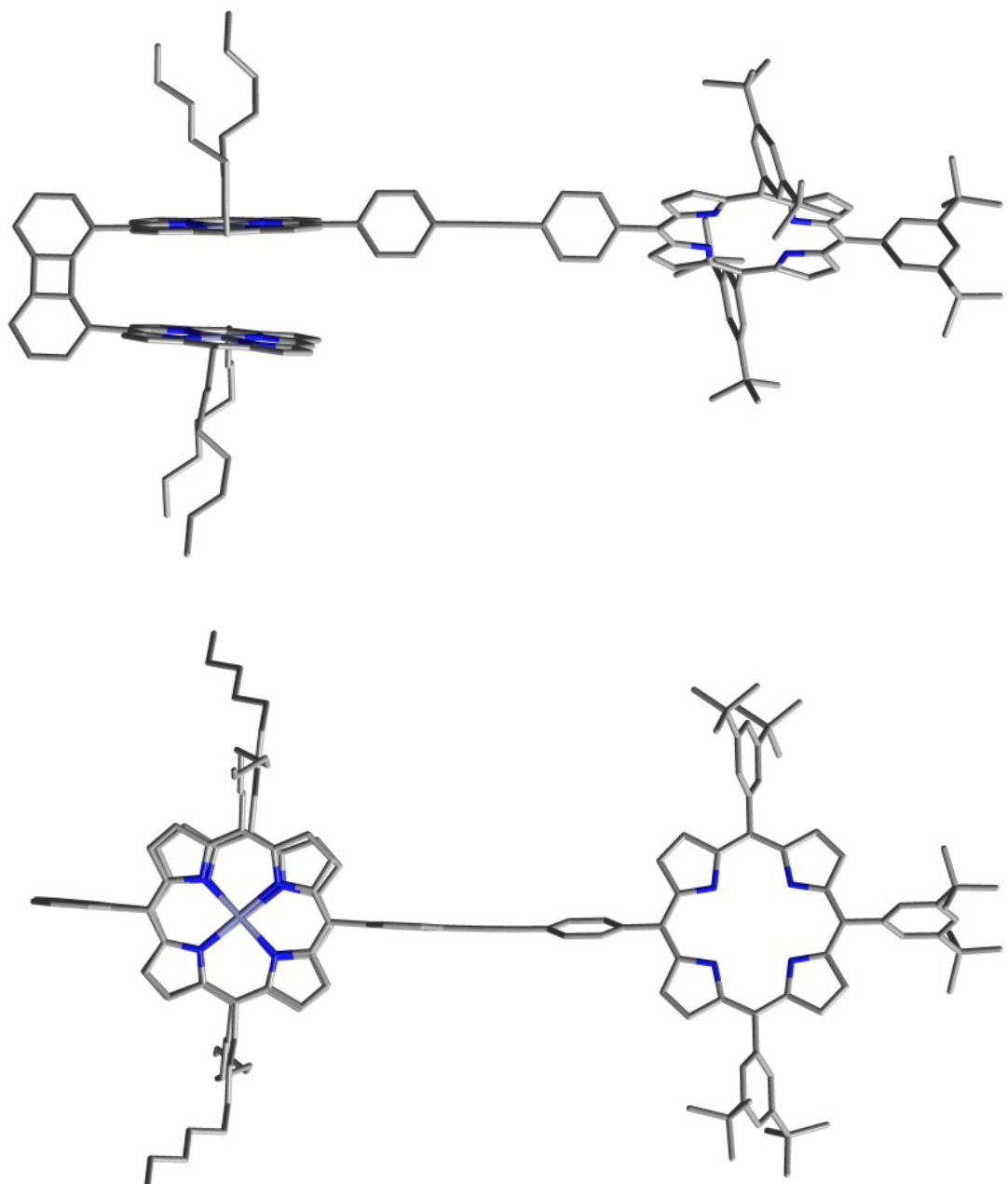


Figure S22. Geometry optimization of **2** (DFT; B3LYP). Top: side view; bottom: top view. The interplanar dihedral angles and center-to-center distances are placed in the text.

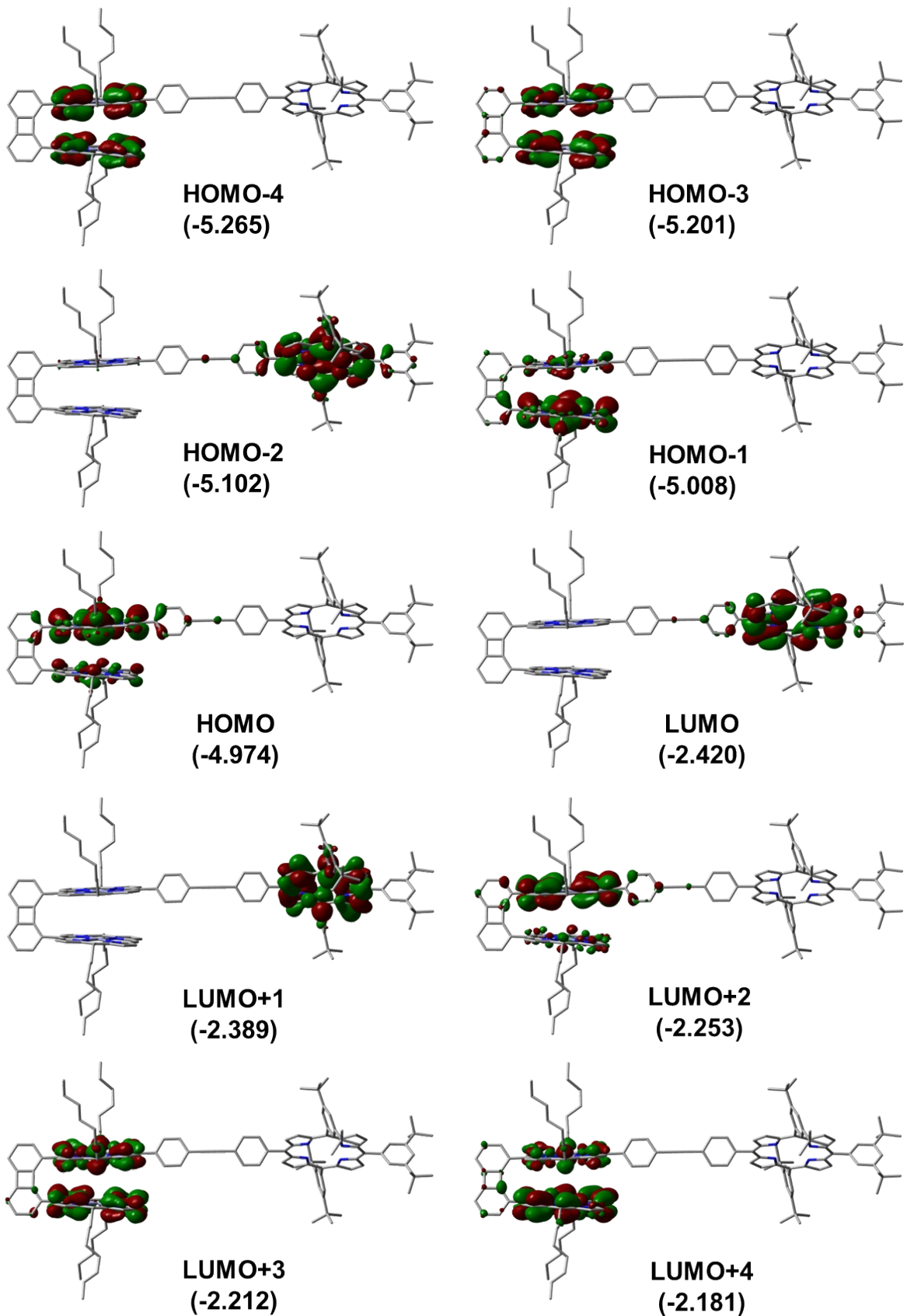


Figure S23. Representation of the frontier MOs of **2**. Energy in eV.

Table S2. Computed positions, major contributions and oscillator strength (f) of the first 100 electronic transitions of **2** (H = HOMO, L = LUMO).

No.	Wavelength (nm)	Osc. Strength	Major Contribs (%)
1	579.3	0.0489	H-5→LUMO (17), H-5→L+1 (15), H-1→LUMO (22), H-1→L+1 (24)
2	552.3	0.0729	HOMO→L+2 (49)
3	548.2	0.0061	H-3→L+2 (15), H-2→L+2 (13), HOMO→L+3 (40)
4	542.8	0.0143	H-2→L+2 (23), H-2→L+3 (16), HOMO→L+4 (12)
5	541.9	0.0627	H-5→LUMO (14), H-5→L+1 (15), H-1→LUMO (20), H-1→L+1 (18)
6	540.0	0.0018	H-2→L+4 (10), H-1→L+4 (10), HOMO→L+4 (25)
7	535.2	0.0003	H-2→L+2 (26), H-2→L+3 (24), HOMO→L+3 (16)
8	529.0	0.0036	H-2→L+4 (33)
9	527.7	0.0053	HOMO→L+4 (13), HOMO→L+5 (48)
10	520.7	0.0073	H-2→L+4 (12), H-2→L+5 (52)
11	496.1	0.0227	H-1→LUMO (17), HOMO→LUMO (71)
12	493.8	0.0057	H-4→L+2 (31), H-4→L+3 (10), H-3→L+2 (30)
13	489.6	0.0057	H-4→L+3 (24), H-4→L+4 (20), H-3→L+3 (29), H-3→L+4 (12)
14	489.5	0.0001	H-1→L+1 (18), HOMO→L+1 (77)
15	485.1	0.0007	H-4→L+2 (10), H-4→L+3 (14), H-4→L+4 (25), H-3→L+5 (37)
16	484.4	0.0021	H-2→LUMO (80)
17	483.9	0.0094	H-4→L+5 (40), H-3→L+4 (33)
18	478.9	0	H-2→L+1 (91)
19	475.3	0.0346	H-1→L+2 (69), HOMO→L+2 (16)
20	468.2	0.0026	H-1→L+3 (73), HOMO→L+3 (16)
21	463.5	0.0011	H-1→L+4 (74), HOMO→L+4 (16)
22	457.4	0.0019	H-3→LUMO (92)
23	456.7	0.0041	H-1→L+5 (74), HOMO→L+5 (17)
24	452.1	0	H-3→L+1 (100)
25	447.8	0.0012	H-4→LUMO (94)
26	442.8	0	H-4→L+1 (100)
27	429.6	0.2234	H-6→L+2 (46), H-4→L+5 (17)
28	424.8	0.0139	H-5→L+2 (89)
29	423.3	0.0322	H-6→L+2 (15), H-6→L+3 (59)
30	419.5	0.2703	H-6→L+2 (10), H-6→L+4 (48)
31	419.1	0.0051	H-5→L+3 (95)
32	415.4	0.0009	H-5→L+4 (99)
33	413.6	0.6694	H-6→L+2 (14), H-6→L+3 (10), H-6→L+4 (38)
34	409.9	0.0013	H-5→L+5 (99)
35	408.5	0.093	H-6→L+5 (53)
36	404.8	0.002	H-6→L+3 (11), H-6→L+5 (36), HOMO→L+6 (10), HOMO→L+7 (14)
37	403.5	1.2397	H-7→LUMO (11), H-5→L+1 (24)
38	398.5	0.0605	H-2→L+6 (24), H-2→L+7 (36)
39	393.3	0.3366	HOMO→L+7 (19)
40	392.9	0.5621	H-5→LUMO (28), H-1→L+1 (12), HOMO→L+6 (14)
41	391.0	0.0247	H-7→LUMO (42), H-6→LUMO (18), HOMO→L+6 (20), HOMO→L+7 (11)
42	389.1	0.0156	H-6→LUMO (69)
43	386.9	0.0311	H-7→LUMO (12), H-6→L+1 (11), H-1→L+6 (24), H-1→L+7 (10), HOMO→L+6 (10)

44	386.2	0.0223	H-6→L+1 (81)
45	382.9	0.0111	H-7→L+1 (60)
46	379.8	0.2936	H-7→L+2 (60)
47	376.0	0.0084	H-8→LUMO (40), H-8→L+1 (41)
48	375.7	0.0245	H-2→L+6 (52), H-2→L+7 (28)
49	373.8	0.0576	H-3→L+6 (32), H-3→L+7 (43)
50	372.4	0.3131	H-7→LUMO (11), H-7→L+1 (13), H-5→L+1 (17), H-1→L+6 (11)
51	371.7	0.1846	H-7→L+2 (11), H-7→L+3 (40), H-7→L+4 (15)
52	369.5	0.1751	H-4→L+6 (25), H-4→L+7 (38)
53	366.4	0.4117	H-7→L+3 (21), H-3→L+6 (11), H-3→L+7 (14)
54	365.0	0.0119	H-11→L+2 (13), H-7→L+3 (12), H-7→L+4 (42)
55	364.9	0.0171	H-12→L+2 (11), H-11→L+2 (27), H-7→L+4 (17)
56	363.1	0.0424	H-12→L+3 (34), H-12→L+4 (12), H-11→L+3 (13)
57	361.3	0.0956	H-7→L+4 (11), H-7→L+5 (42), H-3→L+6 (13)
58	360.6	0.001	H-11→L+3 (19), H-11→L+4 (14), H-11→L+5 (17)
59	360.5	0.2547	H-7→L+5 (15), H-6→L+6 (13), H-6→L+7 (23), H-3→L+6 (13)
60	359.7	0.0043	H-12→L+2 (12), H-12→L+4 (20), H-12→L+5 (22)
61	358.7	0.5649	H-7→L+5 (16), H-4→L+7 (10)
62	358.2	0.0244	H-1→L+6 (23), H-1→L+7 (51)
63	356.4	0.0191	H-8→LUMO (42), H-8→L+1 (43)
64	356.3	0.4325	H-6→L+7 (11), H-3→L+6 (11), H-3→L+7 (17)
65	353.2	0.0832	H-9→L+1 (21), H-5→L+6 (39), H-5→L+7 (17)
66	353.1	0.3595	H-4→L+6 (41), H-4→L+7 (25)
67	351.1	0.1817	H-9→LUMO (71), H-9→L+1 (12)
68	347.8	0.1811	HOMO→L+8 (57)
69	347.6	0.3755	H-9→L+1 (38), H-5→L+6 (17), HOMO→L+8 (13)
70	344.6	0.0108	H-2→L+8 (60)
71	344.3	0.0293	H-16→L+2 (26), H-2→L+8 (18)
72	342.4	0.0255	H-16→L+3 (16), H-10→L+2 (25)
73	340.7	0.0203	H-10→L+2 (14), H-10→L+5 (10)
74	338.5	0.0107	H-17→L+4 (11), H-10→L+3 (24)
75	338.1	0.0093	H-15→LUMO (25), H-15→L+1 (11), H-14→LUMO (46)
76	336.0	0.0545	H-17→L+2 (13), H-13→L+2 (32), H-13→L+3 (11)
77	335.6	0.0432	H-15→LUMO (14), H-15→L+1 (67)
78	333.9	0.0393	H-18→L+1 (24), H-14→L+1 (56)
79	333.1	0.0443	H-13→L+3 (38), H-11→L+3 (10)
80	332.5	0.0165	H-15→LUMO (48), H-14→LUMO (30)
81	332.4	0.0076	H-19→L+3 (12), H-13→L+4 (41)
82	331.1	0.0001	H-12→L+2 (35), H-11→L+2 (16)
83	330.9	0.0023	H-16→L+2 (27), H-10→L+4 (22)
84	330.7	0.0131	H-18→LUMO (70)
85	330.0	0.0239	H-16→L+3 (15), H-3→L+8 (44)
86	329.5	0.0064	H-11→L+3 (24), H-11→L+4 (19), H-10→L+3 (10)
87	329.1	0.0815	H-19→L+2 (12), H-3→L+8 (33)
88	329.0	0.0004	H-5→L+6 (31), H-5→L+7 (69)
89	328.4	0.0311	H-20→L+1 (13), H-18→L+1 (48), H-14→L+1 (15)
90	328.2	0.056	H-17→L+3 (10), H-16→L+3 (12), H-13→L+5 (13)

91	327.7	0.0105	H-17→L+2 (11), H-10→L+4 (10), H-10→L+5 (17)
92	327.2	0.0002	H-12→L+5 (40), H-11→L+4 (20)
93	327.0	0.0101	H-13→L+5 (16), H-12→L+4 (24), H-11→L+5 (33)
94	326.6	0.0003	H-17→L+2 (19)
95	326.2	0.008	H-22→LUMO (29), H-20→LUMO (41)
96	325.6	0.0687	H-20→L+1 (66), H-18→LUMO (10)
97	324.9	0.0007	H-4→L+8 (93)
98	324.1	0.0026	H-17→L+2 (16), H-17→L+3 (14), H-16→L+2 (10), H-16→L+3 (12)
99	323.8	0.0072	H-22→LUMO (16), H-22→L+1 (54), H-1→L+9 (14)
100	322.8	0.0018	H-17→L+4 (10), HOMO→L+10 (44)

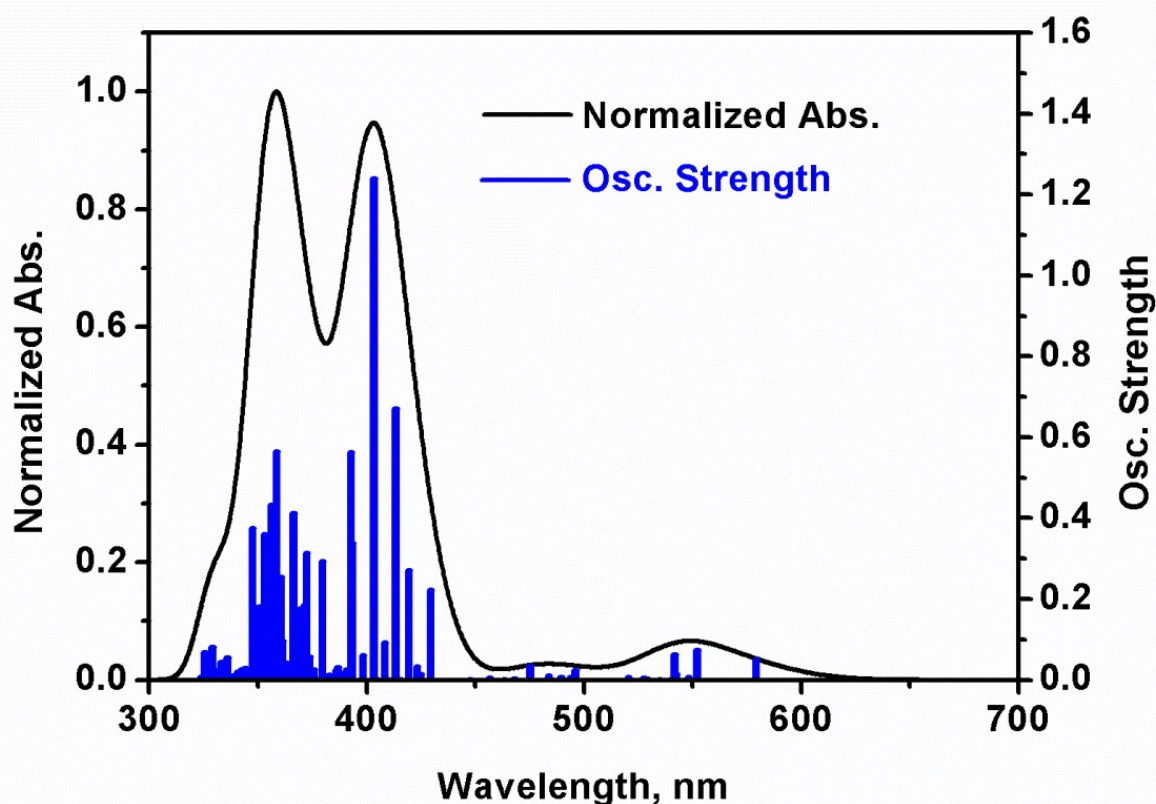


Figure S24. Bar graph reporting the calculated oscillator strength and calculated position of the 100st electronic transitions calculated by TDDFT for **2** (bar graph; f = computed oscillator strength). The black line is generated by assigning an arbitrary thickness of 1000 cm⁻¹ to each bar.

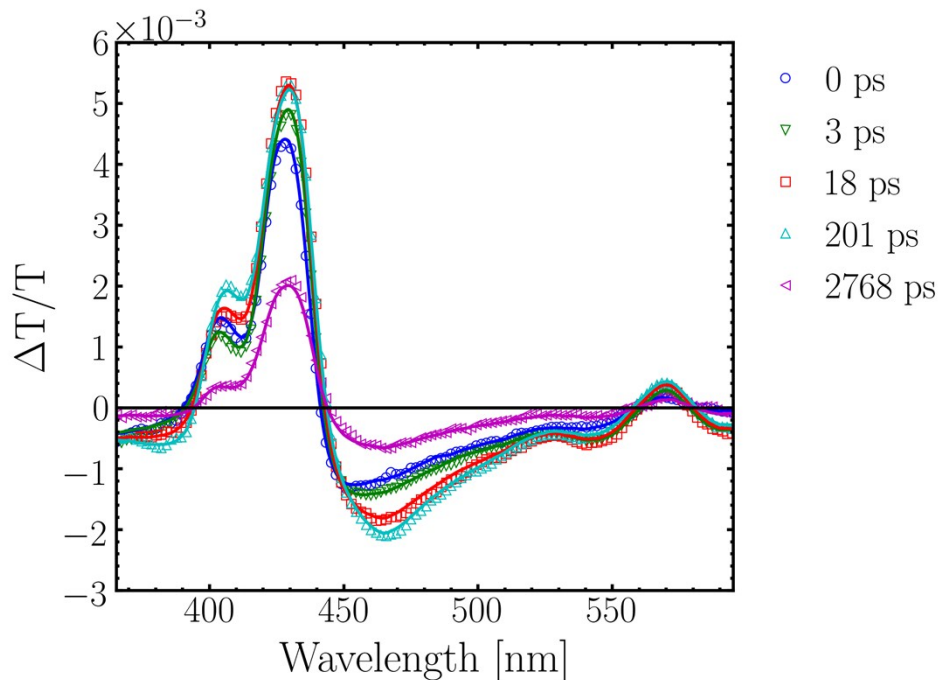


Figure S25. Time evolution of **1** of the fs-TAS in 2MeTHF at 298 K ($\lambda_{\text{exc}} = 425$ nm; 40 pJ/pulse; IRF = 138 fs). The time-deconvoluted spectra (440-600 nm) are in the text.

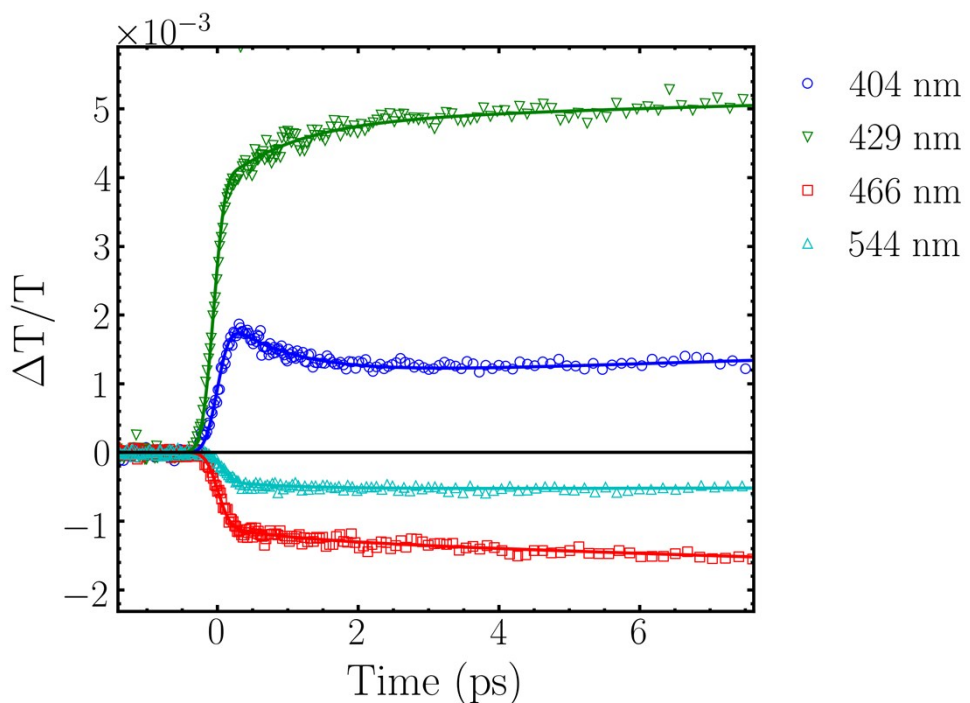


Figure S26. Time evolution of $\Delta T/T$ for **1** in 2MeTHF at 298 K ($\lambda_{\text{exc}} = 425$ nm; 40 pJ/pulse; IRF = 138 fs) for various monitored wavelengths.

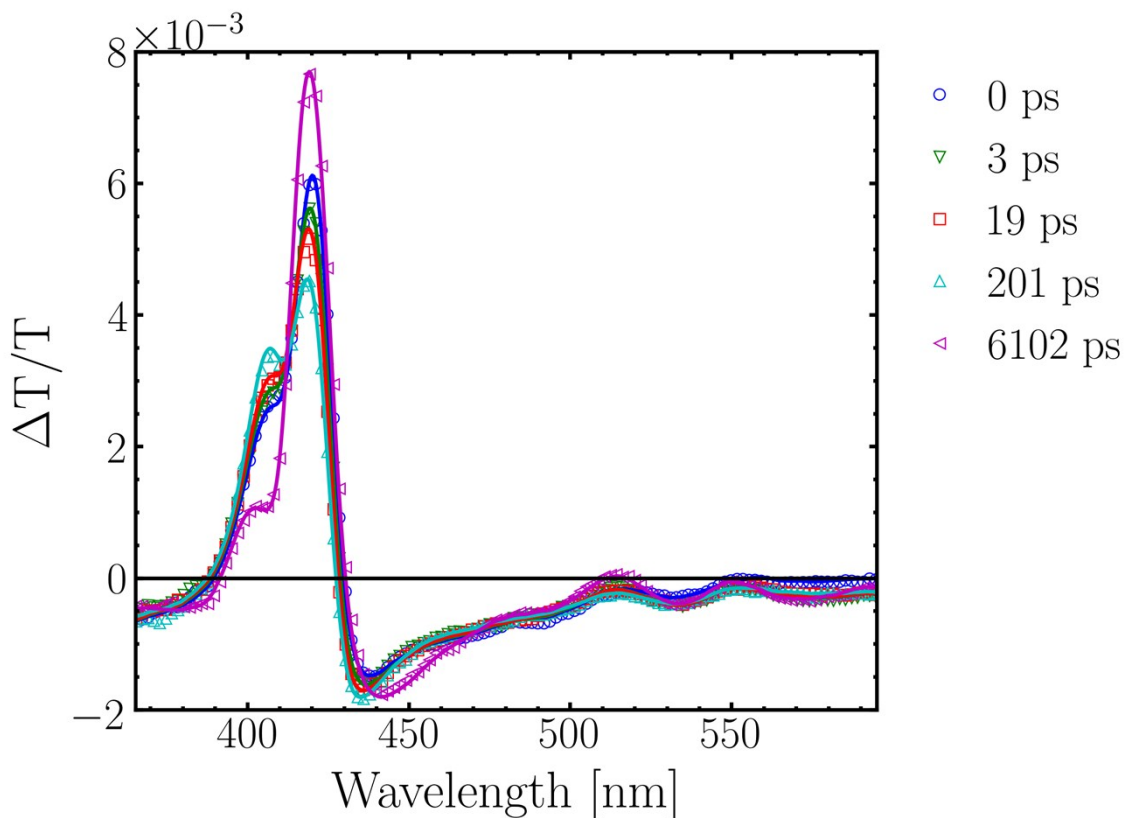


Figure S27. Time evolution of the fs-TAS **2** in 2MeTHF at 298 K ($\lambda_{\text{exc}} = 425$ nm; 40 pJ/pulse; IRF = 160 fs). The time-deconvoluted spectra (440–600 nm) are in the text.

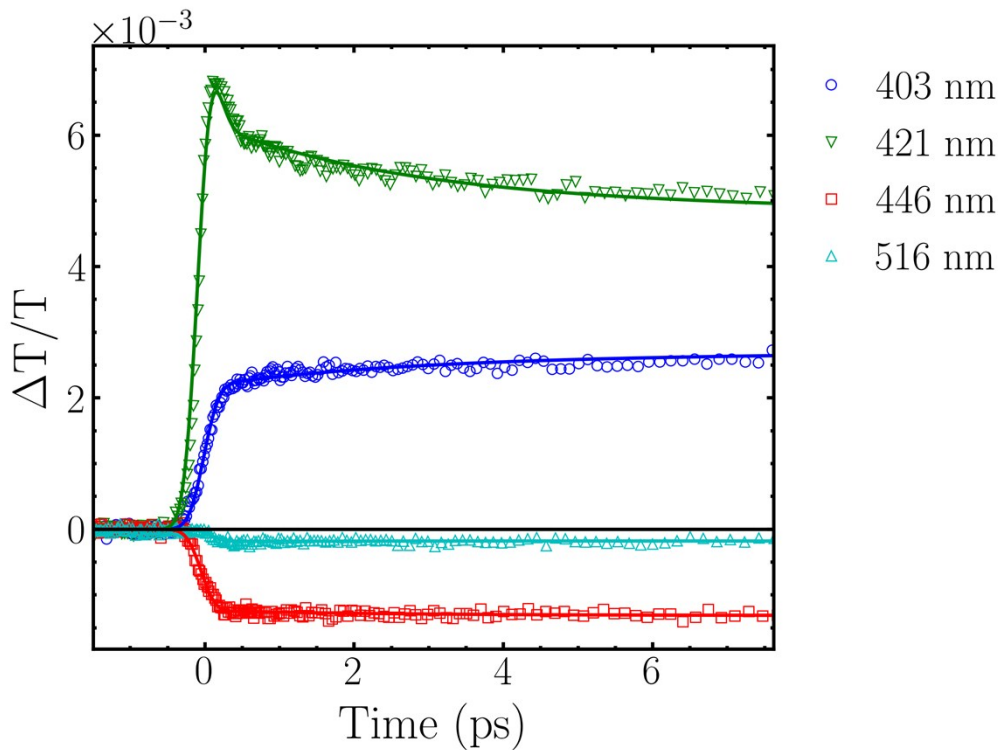


Figure S28. Time evolution of $\Delta T/T$ for **2** in 2MeTHF at 298 K ($\lambda_{\text{exc}} = 425$ nm; 40 pJ/pulse; IRF = 160 fs) for various monitored wavelengths.

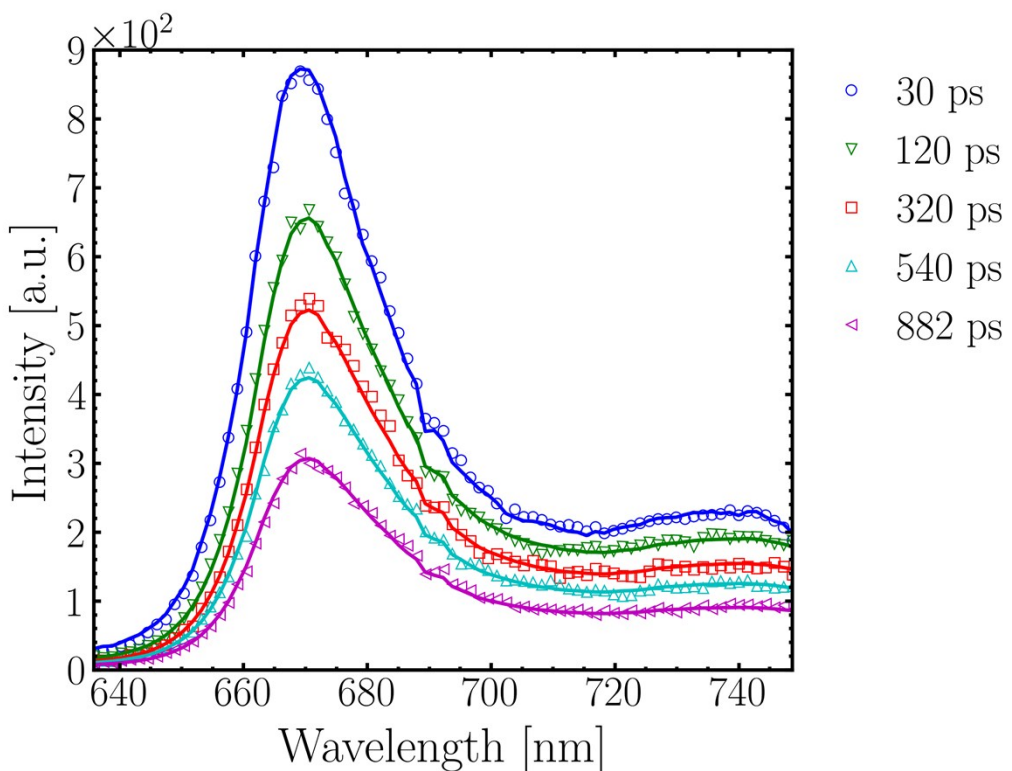


Figure S29. Time evolution of the fluorescence spectra of **1** in 2MeTHF at 298 K (Streak camera, $\lambda_{\text{exc}} = 425$ nm; 500 pJ/pulse; IRF = 10 ps). The time-deconvoluted spectra are in the text.

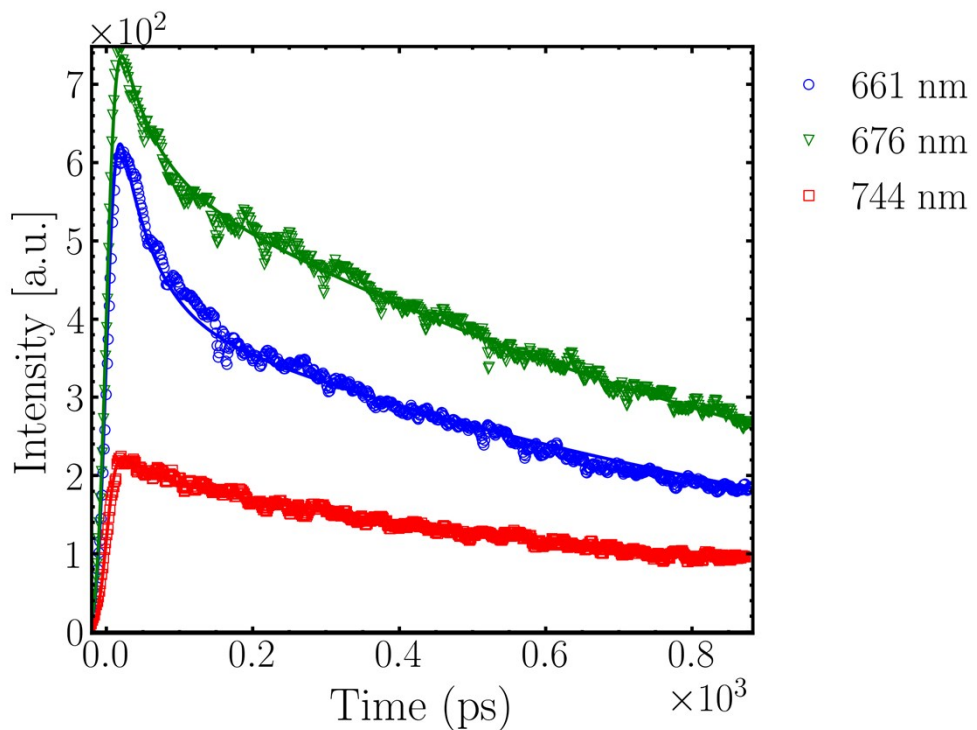


Figure S30. Time evolution of the fluorescence intensity of **1** in 2MeTHF at 298 K monitored at various wavelengths ($\lambda_{\text{exc}} = 425$ nm; 500 pJ/pulse; IRF = 10 ps).

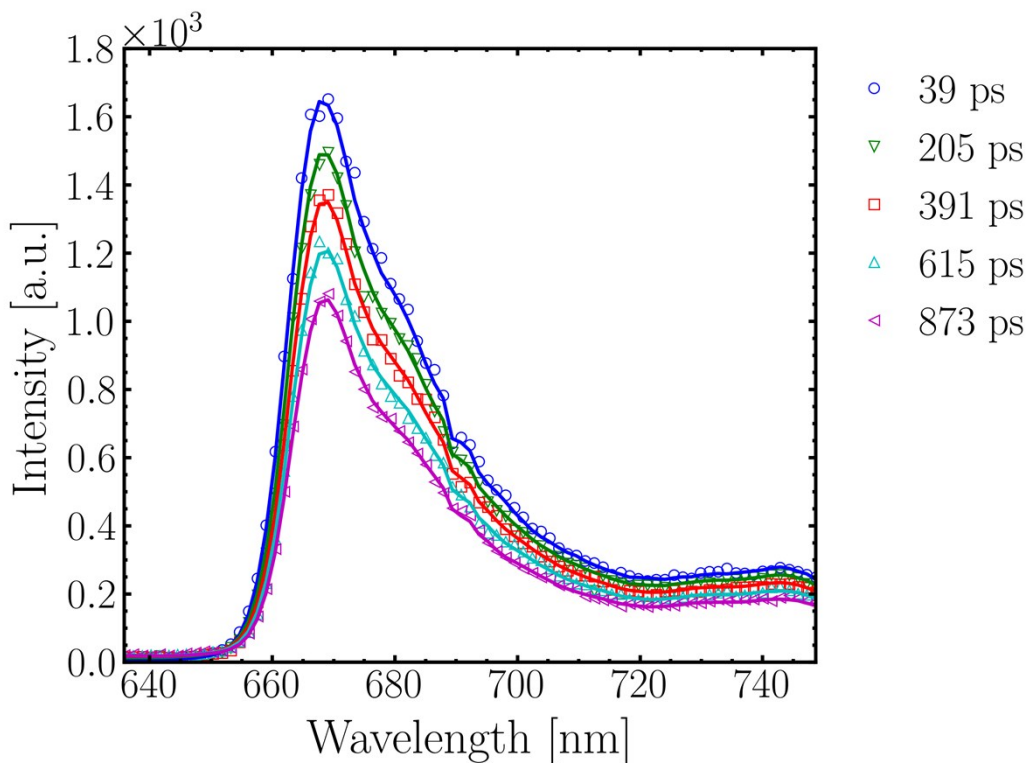


Figure S31. Time evolution of the fluorescence spectra of **1** in 2MeTHF at 77 K (Streak camera; $\lambda_{\text{exc}} = 425$ nm; 500 pJ/pulse; IRF = 11 ps). The time-deconvoluted spectra are in the text.

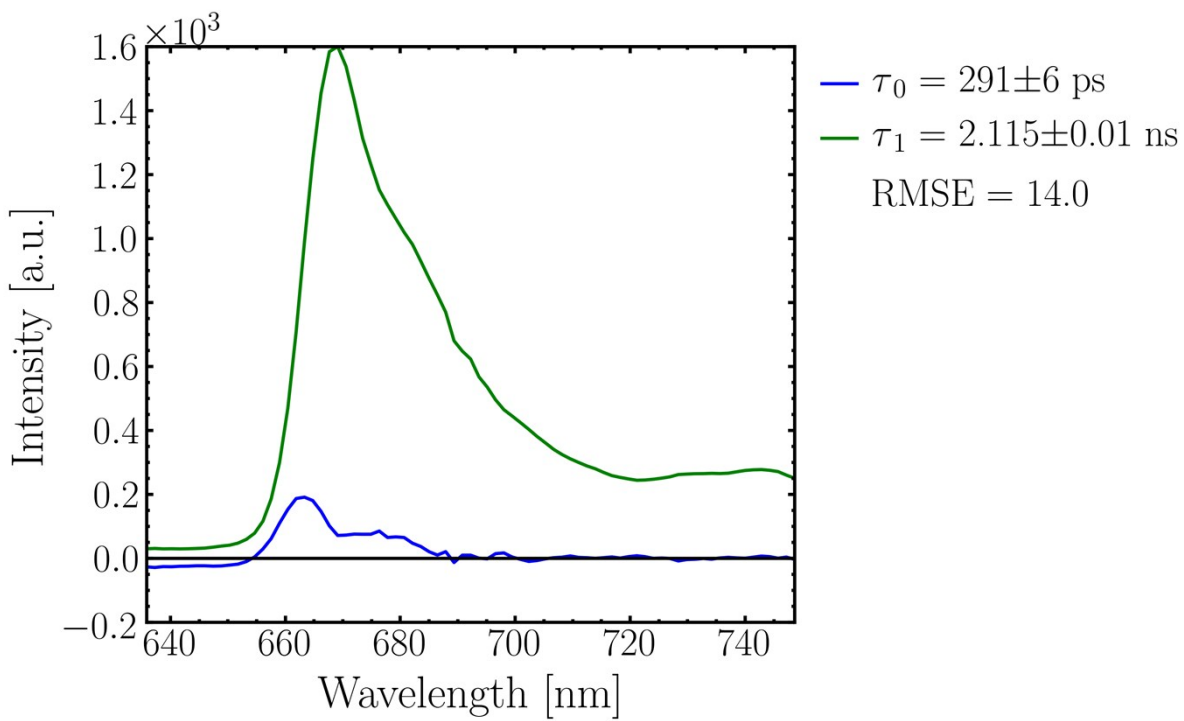


Figure S32. Time-deconvoluted spectra of **1** in 2MeTHF at 77 K. Note that the 2.1 ns value cannot be inaccurate as it exceeds 1 ns, the limit of the Streak camera. Moreover, the shape of the fluorescence of the $[\text{Zn}_2]$ chromophore could not be exact because of the weakness of this component. However, the time scale is.

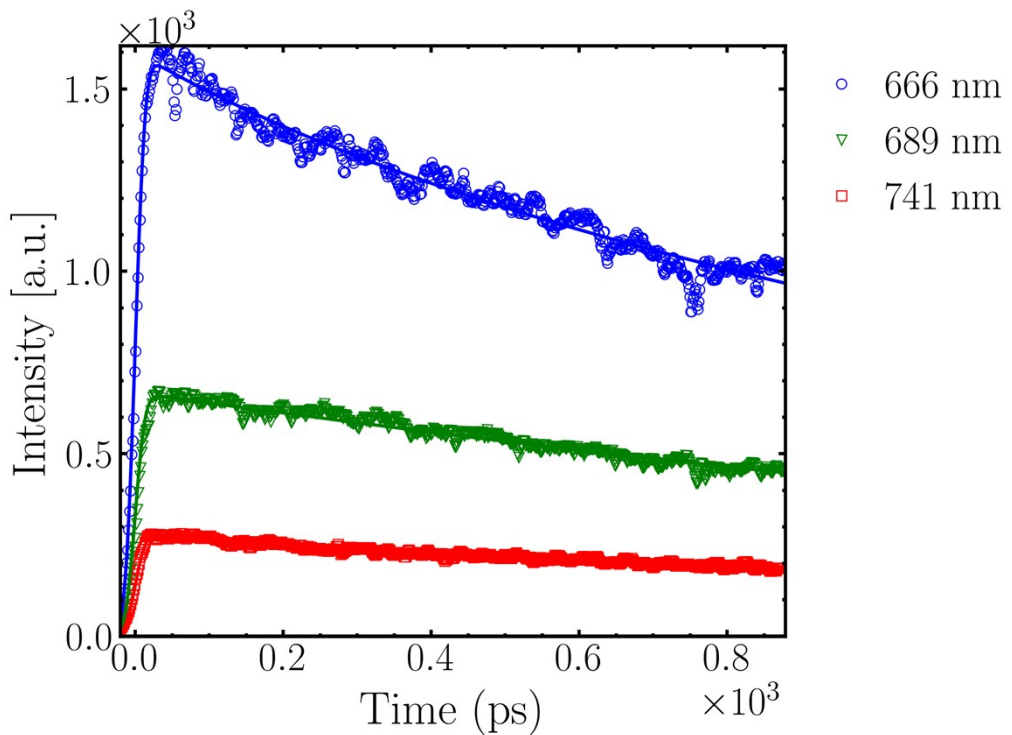


Figure S33. Time evolution of the fluorescence intensity of **1** in 2MeTHF at 77 K monitored at various wavelengths ($\lambda_{\text{exc}} = 425$ nm; 500 pJ/pulse; IRF = 11 ps).

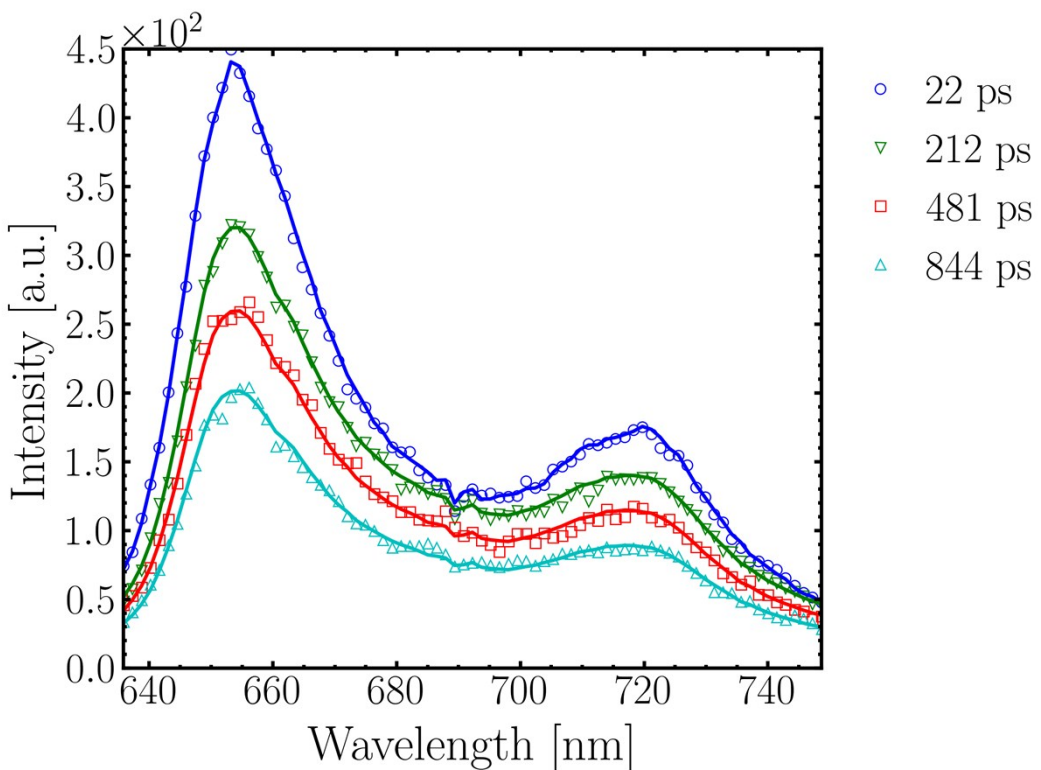


Figure S34. Time evolution of the fluorescence spectra of **2** in 2MeTHF at 298 K (Streak camera; $\lambda_{\text{exc}} = 425$ nm; 500 pJ/pulse; IRF = 10 fs). The time-deconvoluted spectra are in the text.

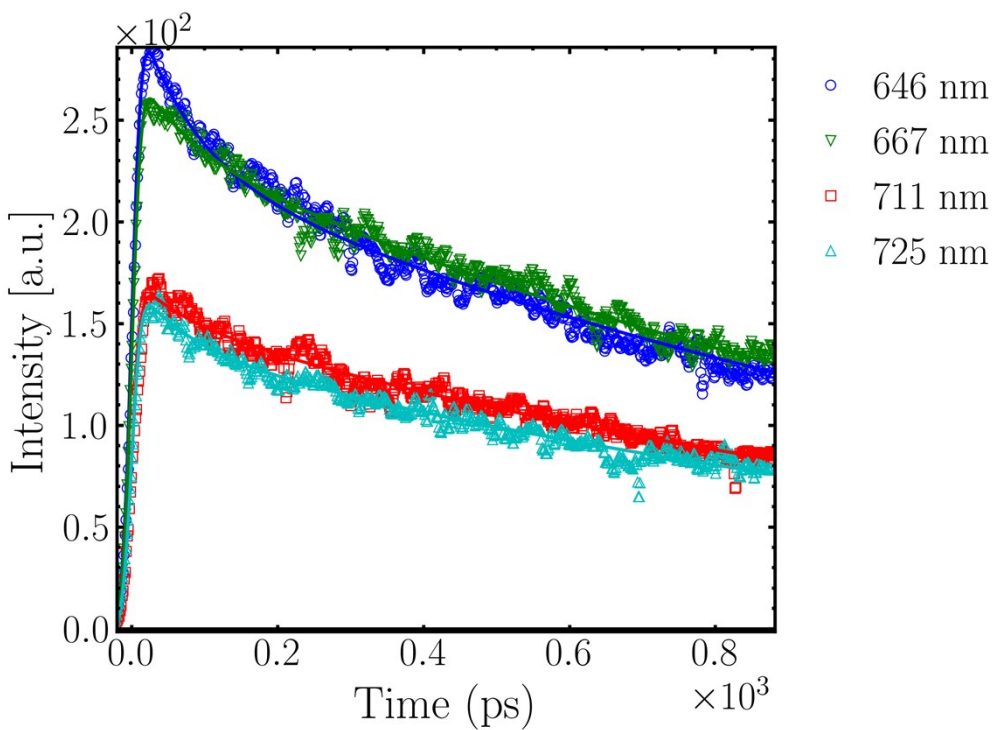


Figure S35. Time evolution of the fluorescence intensity of **2** in 2MeTHF at 298 K monitored at various wavelengths ($\lambda_{\text{exc}} = 425$ nm; 500 pJ/pulse; IRF = 10 ps).

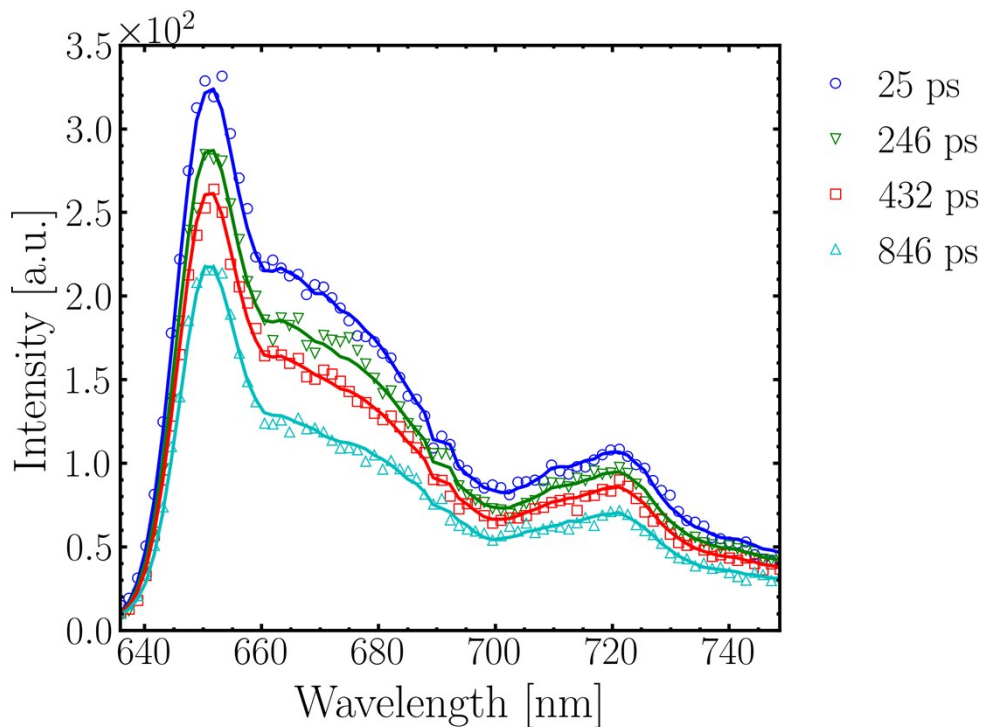


Figure S36. Time evolution of the fluorescence spectra of **2** in 2MeTHF at 77 K (Streak camera; $\lambda_{\text{exc}} = 425$ nm; 500 pJ/pulse; IRF = 10 fs). Note that the 5.5 ns value cannot be inaccurate as it exceeds 1 ns.

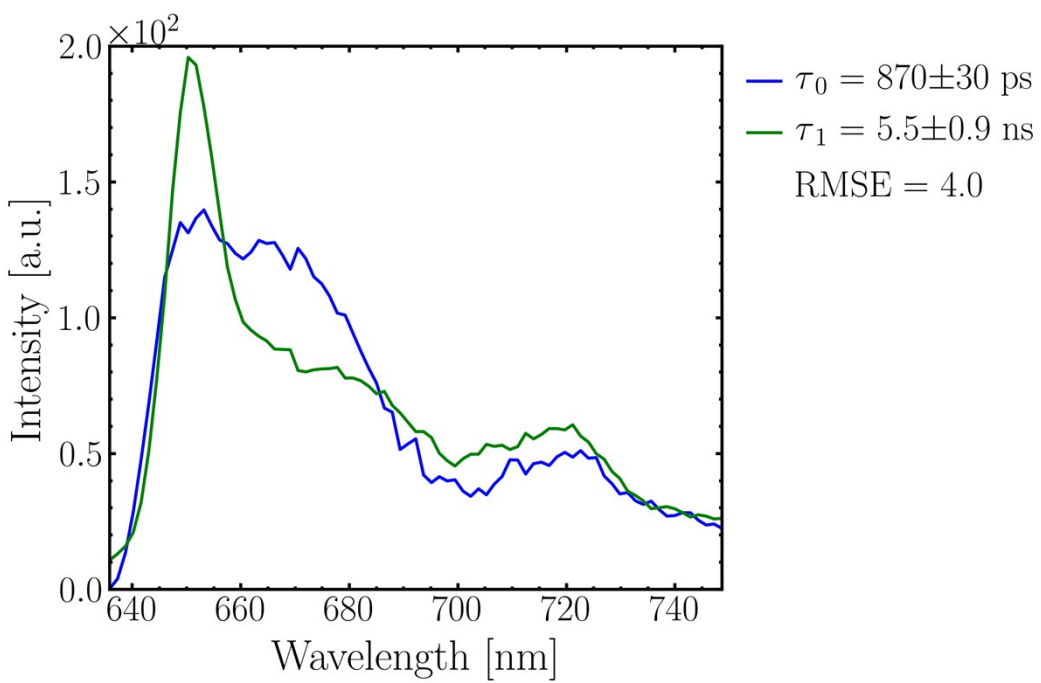


Figure S37. Time-deconvoluted spectra of **2** in 2 MeTHF at 77 K. Note that the 5.5 ns value cannot be inaccurate as it exceeds 1 ns.

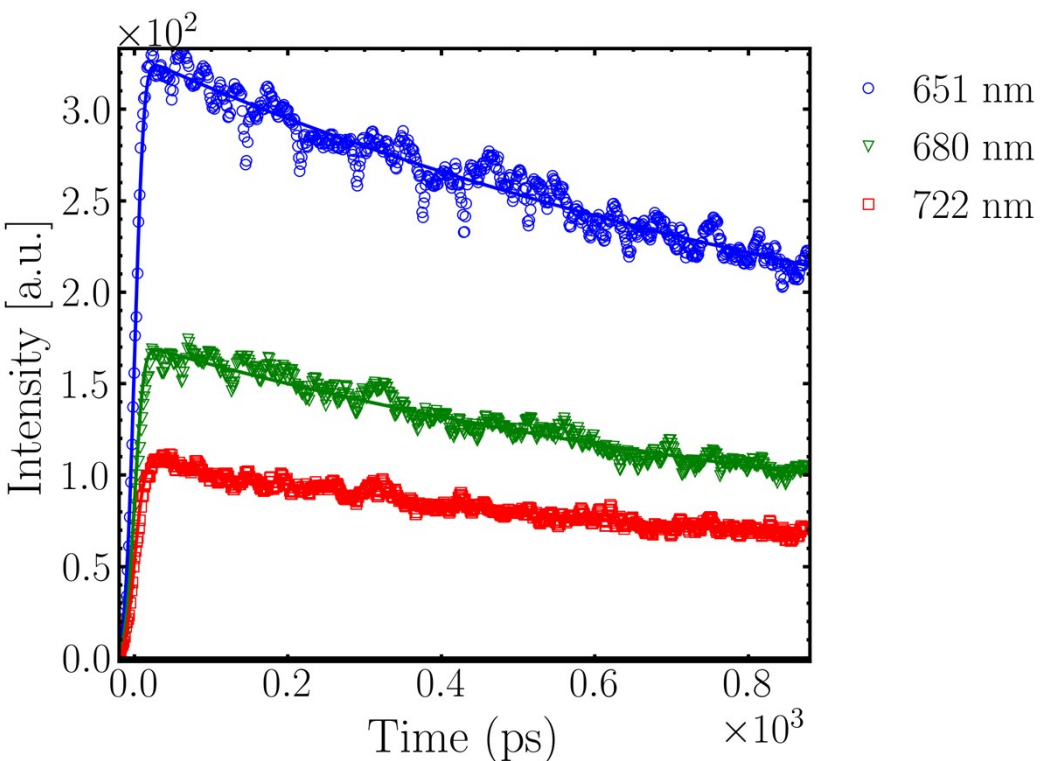


Figure S38. Time evolution of the fluorescence spectra of **2** in 2MeTHF at 77 K monitored at various wavelengths ($\lambda_{\text{exc}} = 425$ nm; 500 pJ/pulse; IRF = 10 ps).

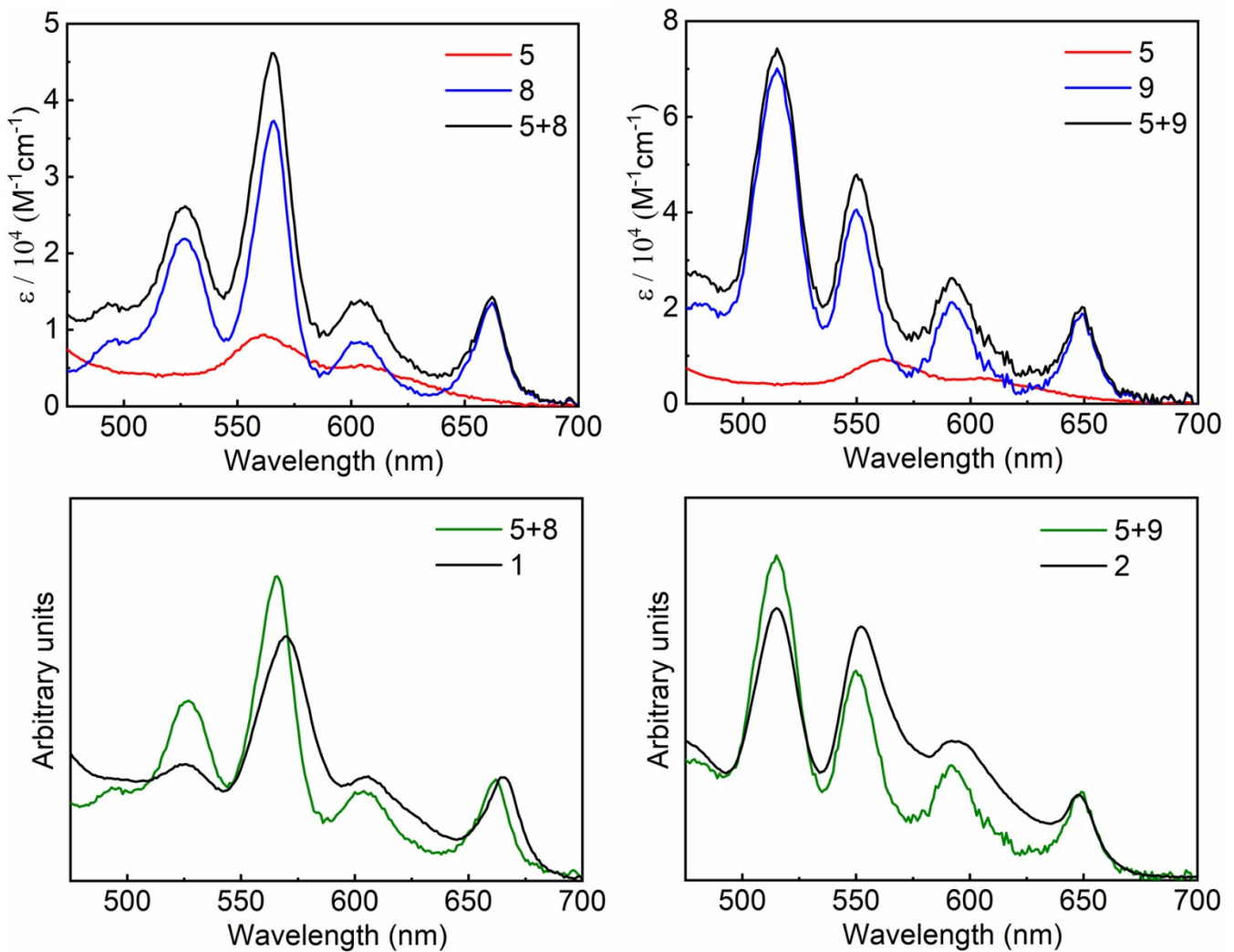


Figure 39. Sum of the absorption spectra of **5 + 8**, and **5 + 9** (top), compared to those for **1** and **2**.

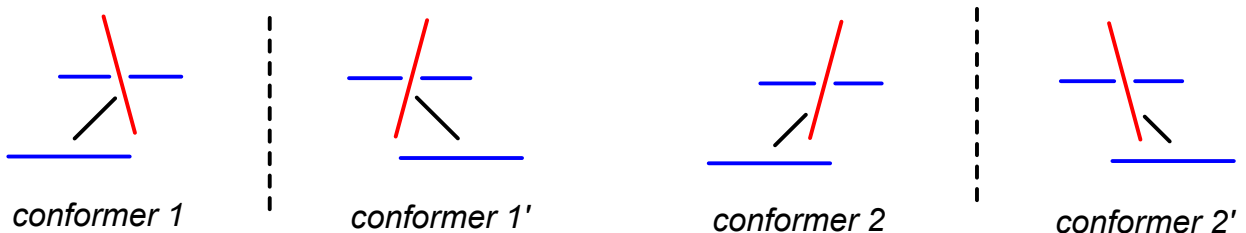


Figure 40. Schematic representations of the four possible conformations of dyads **1** and **2**. Blue = [Zn₂], red = [Fb], black = PDB spacer. For dyad **2**, the bridge C₆H₄-C≡C-C₆H₄, is assumed to be planar ($\gamma = 0^\circ$) for sake of simplicity. Two pairs of conformers are mirror-image of each other.